

this document downloaded from

vulcanhammer.info

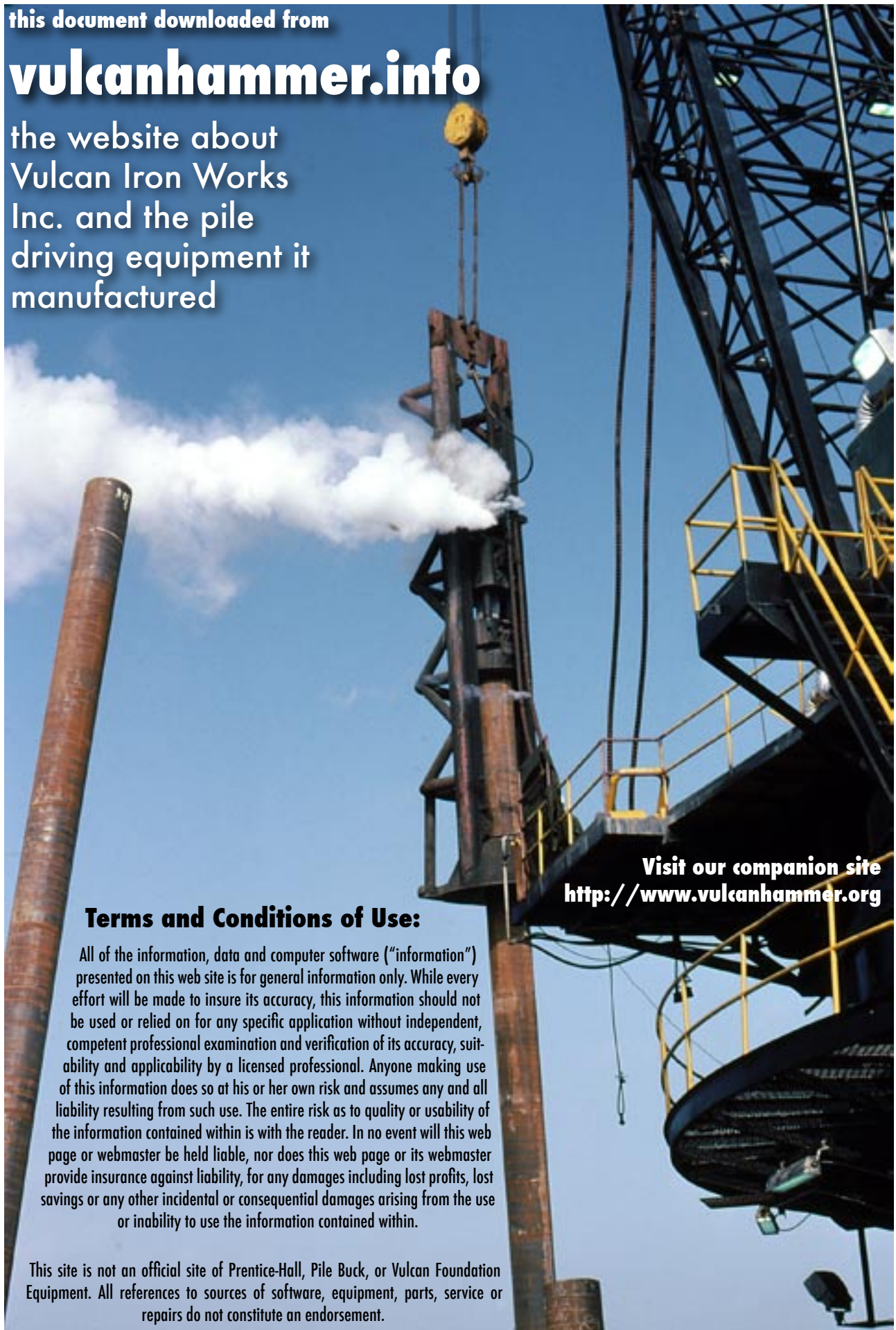
the website about
Vulcan Iron Works
Inc. and the pile
driving equipment it
manufactured

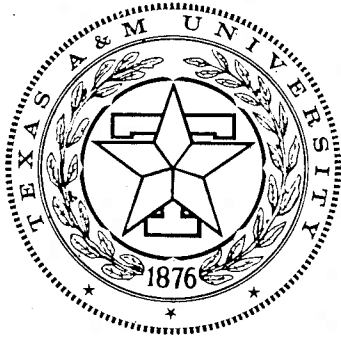
Terms and Conditions of Use:

All of the information, data and computer software ("information") presented on this web site is for general information only. While every effort will be made to insure its accuracy, this information should not be used or relied on for any specific application without independent, competent professional examination and verification of its accuracy, suitability and applicability by a licensed professional. Anyone making use of this information does so at his or her own risk and assumes any and all liability resulting from such use. The entire risk as to quality or usability of the information contained within is with the reader. In no event will this web page or webmaster be held liable, nor does this web page or its webmaster provide insurance against liability, for any damages including lost profits, lost savings or any other incidental or consequential damages arising from the use or inability to use the information contained within.

This site is not an official site of Prentice-Hall, Pile Buck, or Vulcan Foundation Equipment. All references to sources of software, equipment, parts, service or repairs do not constitute an endorsement.

Visit our companion site
<http://www.vulcanhammer.org>





TEXAS
TRANSPORTATION
INSTITUTE

TEXAS
HIGHWAY
DEPARTMENT

COOPERATIVE
RESEARCH

PILE-SOIL SYSTEM RESPONSE IN CLAY
AS A FUNCTION OF EXCESS PORE WATER
PRESSURE AND OTHER SOIL PROPERTIES

in cooperation with the
Department of Transportation
Federal Highway Administration
Bureau of Public Roads

RESEARCH REPORT 33-8
STUDY 2-5-62-33
PILING BEHAVIOR

**PILE-SOIL SYSTEM RESPONSE IN CLAY AS
A FUNCTION OF EXCESS PORE WATER PRESSURE
AND OTHER SOIL PROPERTIES**

by

Tom P. Airhart
Research Assistant

T. J. Hirsch
Research Engineer

Harry M. Coyle
Assistant Research Engineer

Research Report Number 33-8

Piling Behavior Research

Research Study Number 2-5-62-33

Sponsored by

The Texas Highway Department

In cooperation with the

U. S. Department of Transportation

Federal Highway Administration

Bureau of Public Roads

September 1967

TEXAS TRANSPORTATION INSTITUTE

Texas A&M University

College Station, Texas

Preface

The information contained in this report was developed on research study 2-5-62-33 entitled "Piling Behavior" which is a cooperative research study sponsored jointly by the Texas Highway Department and the U. S. Department of Transportation, Federal Highway Administration, Bureau of Public Roads. The broad objective of this project is to fully develop the use of the computer solution of the wave equation so that it may be used to predict driving stresses in piling and also to estimate static load-carrying capacity of piling from driving resistance records.

This report concerns itself with an instrumented field test pile used to investigate the failure mechanisms which are developed in clay soils subjected to pile driving and foundation loadings. The ultimate load response of the pile-soil system was evaluated for both dynamic and static loadings. A test pile instrumented with pressure transducers, strain gages, and accelerometers was driven into a saturated clay at a site in Beaumont, Texas.

Measurements of strains and acceleration of the pile were taken during driving. Pore pressure measurements were made at the pile-soil interface for a continuous period of 30 days after driving. Strain measurements were made during static load tests at 13 days and 30 days after driving. Soil borings were made for the in-situ, remolded, and reconsolidated conditions and at specific radial distances from the pile. Conventional tests were conducted on the soil samples to measure the changes in engineering properties for the different conditions.

The most important single result of this study has been the determination of the mode of failure developed when a steel pile is driven and loaded in a cohesive soil. Both static and dynamic load responses for the pile-soil system considered in this study are a function predominately of the soil properties within the region of local shear failure. The region of local shear failure is in turn a function of the pile diameter.

The opinions, findings, and conclusions expressed in this report are those of the authors and not necessarily those of the Bureau of Public Roads.

TABLE OF CONTENTS

CHAPTER	Page
I. INTRODUCTION.....	1
Nature of the Problem	1
Prior Research.....	1
Purpose and Scope of Research	1
Plan of Research.....	1
II. THEORIES OF SOIL FAILURE.....	2
General	2
Local Shear Failure.....	2
General Shear Failure	3
Proposed Failure Theory Applicable to a Pile Driven Into a Cohesive Soil.....	3
III. PORE WATER PRESSURE FLUCTUATIONS ASSOCIATED WITH A PILE DRIVEN INTO A SATURATED COHESIVE SOIL	5
General	5
Theory of Reese and Seed.....	5
Theory of Soderberg.....	6
Proposed New Theory.....	6
IV. STATIC AND DYNAMIC RESPONSE TO LOADING OF THE PILE-SOIL SYSTEM	8
General	8
Nature of Dynamic Response	8
Nature of Static Response	9
V. PILE FABRICATION AND INSTRUMENTATION.....	9
The Pile and Its Fabrication	9
Instrumentation	11
VI. LABORATORY AND FIELD SOIL TEST AND SAMPLE PROCEDURES	12
Soil Profile and Identification Data	12
Field Sampling Procedures	13
Laboratory Test Procedures.....	14
VII. OBSERVATIONS OF SOIL DISTURBANCES	14
Pore Pressure Measurements Related to Soil Disturbance	14
Soil Property Measurements Related to Soil Disturbance	14
Observation of Soil Structure Disturbance by Means of X-ray Absorption Techniques	17
VIII. PORE WATER PRESSURE FLUCTUATIONS ASSOCIATED WITH SOIL FAILURE	18
Measurements Taken After Driving.....	18
Measurements Taken After Static Load Tests	19
IX. RESPONSE OF THE PILE-SOIL SYSTEM TO STATIC AND DYNAMIC LOADING	21
Total Response during Driving.....	21
Static Load Response Changes with Time.....	23
X. CONCLUSIONS	24
XI. RECOMMENDATIONS	25
Practical Applications of Study Results	25
Suggestions for Further Research.....	25
REFERENCES.....	26
APPENDICES.....	28
A. Soil Property Data	
B. Pore Pressure Data	
C. Load Transfer Data	
D. Records of Pile Test Loading and Driving	
E. Computer Simulation	

LIST OF FIGURES

Figure		Page
2.1	Local Shear System	2
2.2	Local Shear Disturbance from Soderberg (31)	3
2.3	General Shear Failure of Terzaghi	3
2.4	General Shear Failure of Meyerhof	3
2.5	General Shear Failure of Rapid Single Stroke Penetration	4
2.6	General Shear Failure Generated by Driving Pile into Saturated Cohesive Soil	4
2.7	Soil Failure Adjacent to Pile	4
3.1	Initial Pore Pressure Patterns from Soderberg (31)	6
5.1	Test Pile	9
5.2	Diesel Hammer	9
5.3	Welding Open End Segment	10
5.4	Instrument Location	10
5.5	Instrument Leads	10
5.6	Pressure Transducer Installation	10
5.7	Strain Gage Leads and Pressure Transducer Installation	11
5.8	Accelerometer Installation	11
5.9	Access Port	12
5.10	Location of Instruments around Pile Wall	12
6.1	Soil Profile	13
6.2	Drill Rig	13
6.3	Performing Vane Shear Test at Field Site	13
7.1	Initial Pore Pressure Dissipation 50' Depth	14
7.2	Vane Shear Strengths	15
7.3	Unconfined Shear Strength	15
7.4	Dry Unit Weights	15
7.5	Moisture Contents	15
7.6	Consolidation Curves—40' Depth	16
7.7	Radiogram 40' Depth	16
7.8	Radiogram 15' Depth	17
8.1	Pore Pressure Measurements in Clay Stratum—50' Depth	18
8.2	Pore Pressure Measurements in Clay Stratum—40' Depth	18
8.3	Pore Pressure Measurements in Sand Stratum—30' Depth	18
8.4	Initial Pore Pressure Dissipation in Clay Stratum—50' Depth	19
8.5	Initial Pore Pressure Dissipation in Clay Stratum—40' Depth	19
8.6	Excess Pore Water Pressure due to Static Load Test #1—50' Depth	19
8.7	Excess Pore Water Pressure due to Static Load Test #2—50' Depth	19
8.8	Excess Pore Water Pressure due to Static Load Test #3—30' Depth	20
8.9	Excess Pore Water Pressure due to Static Load Test #4—30' Depth	20
8.10	Peak Pore Pressures Reached after Static Load Tests	20
8.11	Pore Pressure Dissipation in Clay Stratum after Load Test—50' Depth	20
8.12	Pore Pressure Dissipation in Clay Stratum after Load Test—40' Depth	20
9.1	Field Measurements of Acceleration Integrated to Displacements	21
9.2	Corrected Measurements of Acceleration Integrated to Displacements	22
9.3	Maximum Dynamic Soil Resistance upon Each 5 ft. Segment	22
9.4	Static Load Test Equipment	23
9.5	Load Transfer Curves 13 Days after Driving—Test #1	23
9.6	Load Transfer Curves 13 Days after Driving—Test #2	23
9.7	Load Transfer Curves 30 Days after Driving—Test #1	24
9.8	Load Transfer Curves 30 Days after Driving—Test #2	24

Pile-Soil System Response in Clay as a Function of Excess Pore Water Pressure and Other Soil Properties

CHAPTER I

INTRODUCTION

Nature of the Problem

The response of soils to static load systems has been explored for some years primarily because such systems are encountered frequently in practice. On the other hand, response to dynamic load systems is becoming a pressing matter with the advance of technology, thus dictating attention. A typical example concerns the interaction of a pile during the driving operation and its supporting soil. Often ignored in the application of equations of applied mechanics to the description of soil failures is the complex nature of soil as an engineering material. Soils, as opposed to manufactured engineering materials, are subject to change in engineering properties both with load application and time. This requires adjustment of the complex soil structure to the new environment created by the applied load. Large discrepancies often occur between full scale load test capacities and those calculated by existing theories. This is particularly true when the parameters for the theoretical calculations are not well defined. Progress has been made in soil mechanics research and practice toward development of sampling and laboratory test techniques for establishing engineering properties of soils in nature. It is considered that more effort should now be made toward the determination of modes of soil response and ultimate failure mechanisms as a function of soil conditions which may vary with time and manner of load application.

Prior Research

Many authors have investigated the modes of soil response and ultimate failure mechanisms associated with dynamic and static foundation loadings. Much of the pioneer work in this area was accomplished by Terzaghi (34),* who proposed modes of soil response to vertical and horizontal static loading for foundations of various depths. The basic concepts of Terzaghi have been extended by Meyerhof (20) to better describe observed behavior in the field. Similarly, efforts have been made toward investigation of the dynamic response of soils. Both Terzaghi (34) and Timoshenko (37) investigated the elastic response of soil subjected to periodic motions imposed by flat slabs. Analysis of the same case has been extended by Reissner (26) and Pauw (23) to include the effect of soil mass upon this type of response. Investigations into the elastic response of soils when subjected to various types of pile loadings have been conducted by Chellis (7) and Barkan (1). Soil response during driving of a pile into a soil medium has

been studied in relation to its effect upon the stresses developed in piling (13) (27) (28) (15) (16) (34).

Purpose and Scope of Research

The purpose of this study was to present a general concept of the development of failure mechanism in soils *Numbers in parentheses indicate references listed near end of report. subjected to pile foundation loadings. The adequacy with which the theories of applied mechanics describe the failure mechanism developed in a pile-soil system was evaluated by measuring soil disturbances and mechanical responses of the pile. The ultimate load response of the pile-soil system developed within this failure mechanism was evaluated for both dynamic and static loadings.

Plan of Research

In order to accomplish the objectives of this research, a test pile instrumented with pressure transducers, strain gages, and accelerometers was driven into a saturated clay soil and instrument measurements were recorded. Conventional static and a few newly developed dynamic soil tests were performed upon soil samples obtained at specific radial distances from the pile. The purpose of the conventional tests was to measure changes in the engineering properties of the soil when subjected to various states of disturbance. Direct observations of soil structure disturbance were obtained by means of X-ray absorption techniques.

Since the number of borings was limited, due to their interference with other tests, indirect measurements of soil disturbances due to driving were obtained by measurement of pore water pressures at the pile surface. The purpose of such measurements was to determine the mathematical model most accurately describing field pore water pressure dissipation patterns as a function of various magnitudes and dimensional extents of soil disturbances due to driving. Pore pressure observations were also used as an indication of soil disturbances associated with static loading to failure.

Measurements of strains and accelerations of the pile were made during driving. They were used in conjunction with a computer program simulating the physical system in order to obtain a measurement of the magnitude and distribution of the dynamic soil response during driving. Readings of strain were used during static load tests, performed approximately two and four weeks after driving, in order to evaluate the changes in magnitude and distribution of static soil response with time.

CHAPTER II

THEORIES OF SOIL FAILURE

General

Failure of soils is usually classified in the literature as falling into two categories: local shear and general shear failures (34). Individual cases of failure are classified according to total load transmitted, time rate of deformation occurring prior to failure, general type of foundation, and soil properties. A failure mode ranging from local to general shear failure is assumed for a specific case, and a theoretical load bearing capacity calculated according to the mathematical analysis of the assumed failure. The various mathematical analyses describing shear failures encompass varying dimensional extents of material involved in the ultimate load response of the foundation soil system. It is proposed in this report that the terms local and general shear failure be differentiated according to the effect produced by such failure upon the structure of the soil. It is further proposed that, in general, complete failure of soils is a combination of these two types of shear failure. The relative extent of each of these two types of shear failure within the complete failure mechanism is determined by the engineering properties of the soil. The over-all dimensional extent of the soil involved in the failure mechanism is intimately associated with the susceptibility of the particular soil involved to volume change during the time interval of load application.

Soils may be classified into two broad categories: cohesionless and cohesive (32). Cohesionless soils, such as sands, exist in a state of direct particle contact. Cohesive soils, such as clays, possess a layer of moisture about each particle that is bound to it by electrostatic charge of the particle. In the unconsolidated state the bound layers of water serve as the interparticle contacts of the randomly oriented clay particles. As consolidation progresses and free water is moved out, the particles displace the layers of bound water and bear more directly upon each other in a denser arrangement. These layers of bound moisture impart to clay soils many of their unique properties (5) (2) (14).

Another factor which must be considered in the loading of saturated soils is the effect of free water contained in the voids between the soil particles. Due to the impermeable nature of clay soils and the short time duration of dynamic loadings, this free pore water is, during loading, trapped within the confines of its local void. Load transfer is then accomplished by the soil particle-pore water system. The response of a saturated clay subjected to loading was first envisioned by Terzaghi (34). According to his consolidation theory, when a clay is initially loaded, practically all of the imposed load is transferred to the incompressible pore water. The resulting pressure in the pore water causes flow away from the immediate regions of load application. Equalization of pressure with the surrounding medium produces a migration of a volume of pore water from this region. The soil particle structure assumes a denser arrangement and supports the imposed load. The time required for the attainment of this denser arrangement is a function of the permeability of the soil. Terzaghi referred to this process of slow change in soil structure and pore water dissipation as consolidation.

He found a change in the engineering properties of the soil associated with this consolidation (32).

This same process occurs within the short time intervals of dynamic load application. In such cases the soil may fail locally with large relative movements of particles resulting in a completely disrupted particle structure, or, it may yield as a mode of general displacement in the form of large translations of the undisturbed soil structure. The soil structure in this latter case moves as a unit with only minute relative movements between particles. Thus, a local shear failure would result in a new soil particle arrangement with greatly altered engineering properties. Soil involved in a general shear failure would experience little change in its engineering properties.

Local Shear Failure

The interaction of these two types of yield may be described analytically by the theories of elasticity and plasticity. The region of local shear failure developed immediately adjacent to the pile is the result of horizontal pressures and displacements due to the insertion of the pile into a position previously occupied by a soil volume. Further disturbance results from vertical shear and displacement occurring as the pile moves through the soil with each hammer blow. It is visualized that a given region of soil is brought to a complete plastic failure by the horizontal forces, then displaced while in this condition by the vertical forces. The dimensional extent of these deformations away from the pile-soil interface is greater than could be explained by sliding friction alone. The conditions governing the dimensional extent of local plastic yield in the soil can be computed by applying the theories of elasticity and plasticity (37) (10) (22). The physical system is shown in Figure 2.1. The region undergoing local shear failure

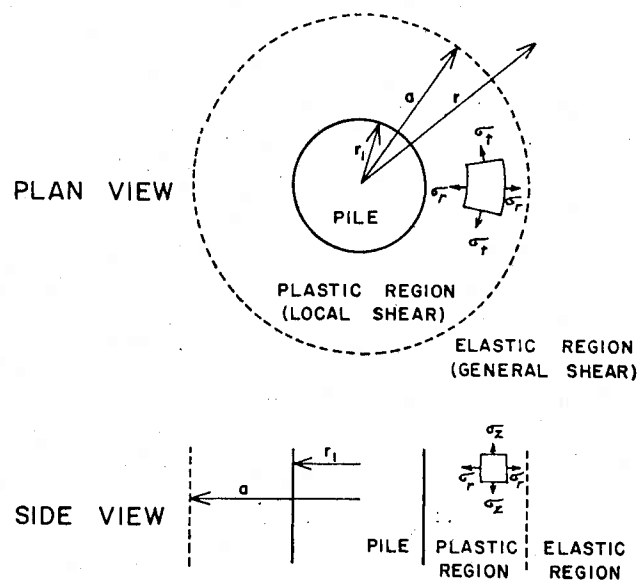


Figure 2.1 Local shear system.

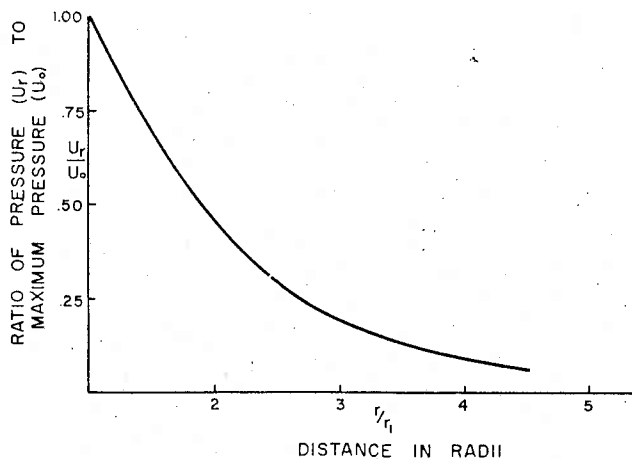


Figure 2.2. Local shear disturbance from Soderberg (31).

corresponds to the region in the plastic state as presented in applied mechanics texts. The region in general shear failure corresponds to the material in the elastic state. Nadai (22) has presented the analytic solution for the stresses developed in such a system. In simplified form, (based on constant volume assumption) stresses developed in the region of local shear failure $r \leq a$ are:

$$\sigma_r = -\frac{\sigma_0}{\sqrt{3}} \left(1 + 2 \ln \frac{a}{r} \right) \quad (2.1)$$

$$\sigma_t = \frac{\sigma_0}{\sqrt{3}} \left(1 + 2 \ln \frac{a}{r} \right) \quad (2.2)$$

$$\sigma_z = -\frac{2\sigma_0}{\sqrt{3}} \left(\ln \frac{a}{r} \right) \quad (2.3)$$

where: σ_0 = yield stress in pure tension

σ_r = radial stress

σ_t = tangential stress

σ_z = axial stress

r = variable radial distance

a = radial extent of local shear disturbance

Stresses in the elastic region, or the region of general shear failure $r \geq a$ are:

$$\sigma_r = -\frac{\sigma_0}{\sqrt{3}} \cdot \frac{a^2}{r^2} \quad (2.4)$$

$$\sigma_t = -\frac{\sigma_0}{\sqrt{3}} \cdot \frac{a^2}{r^2} \quad (2.5)$$

$$\sigma_z = 0 \quad (2.6)$$

Soderberg (31) has applied Nadai's solution to the case of local shear failure in the soil around a pile and determined the relative pressures and radial extent of disturbance according to this theory to be as shown in Figure 2.2.

General Shear Failure

Alternate approaches to the dimensional extent of soil disturbed in general shear failure under static load

have been presented in the literature. One approach is based upon the Mohr shear strength theory (21). According to this theory, failure occurs when the ultimate shear strength of the material in the vicinity of the pile surface is reached. Extensions of this theory increase the allowable ultimate bearing capacity by recognizing the effects of overburden pressure. One of the first true recognitions of general shear failure was presented by Terzaghi (34). He utilized the theory to describe a yield mechanism at the base of the foundation. Further, there was superimposed a surcharge upon this failure mechanism equal to the weight of the overlying material as shown in Figure 2.3. More recently, Meyerhof (20) has presented a mathematical extension of Terzaghi's basic failure mechanism. The mode of failure envisioned by Meyerhof's approach is as shown in Figure 2.4. A concept for a special circumstance of general shear failure has been developed by Thompson (36) for the case of extreme high speed penetration of missiles. The Thompson concept envisions a mode of failure as shown in Figure 2.5. Mechanisms of failure have been observed in both model and full scale tests carried out by Thompson which tend to verify his theory in the case of high speed, frictionless, single stroke penetrations.

It can be noted by careful examination of these various theories of general shear failure that the dimensional extent of the failure mechanism developed depends upon the susceptibility of the material to volume change during the period of load application. The relation of the dimensional extent of the general shear failure as a function of the susceptibility of the material to volume loss permits a possible explanation for the very high bearing capacities of dense cohesionless materials. If a greater volume is brought into the engineering response of the soil in the form of general shear failure than that envisioned by current theories, then a higher load carrying capacity may be developed than predicted by these theories.

Proposed Failure Theory Applicable to a Pile Driven Into a Cohesive Soil

If all aspects of soil structure change and pore water pressure response of a pile-soil system are considered, a model of the failure mechanism can be formulated. It is proposed that the susceptibility of a saturated clay to volume change during short time intervals

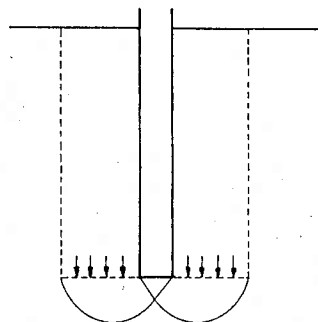


Figure 2.3 General shear failure of Terzaghi.

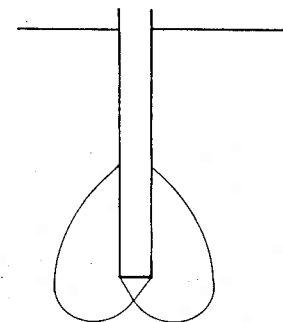


Figure 2.4. General shear failure of Meyerhof.

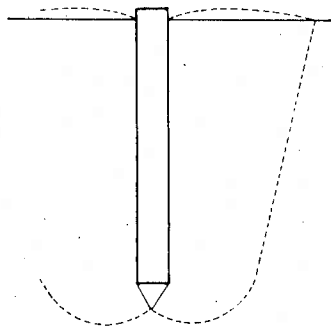


Figure 2.5. General shear failure of rapid single stroke penetration.

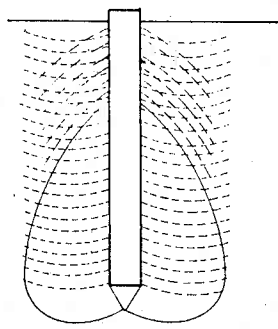


Figure 2.6 General shear failure generated by driving pile into saturated cohesive soil.

of dynamic load applications encountered in pile driving will result in the development, with each hammer blow, of a failure mechanism involving a certain volume of soil. The dimensional extent of shear failure will vary with particular soils and rates of load application, but will develop in general according to Figure 2.6. While the shear failure mechanism thus developed results from point load application, a very important part of the load response of a pile driven into a clay develops along the length of pile in the form of surface friction.

As shown in Figure 2.7, the greatest relative movement occurring in the soil along the length of a pile, as it is driven into the ground, takes place a short distance from the surface of the pile within the region of local shear failure. The soil is forced from its natural state, to a denser arrangement in the zone of local shear failure. This alteration is due initially to the disturbance about the passing tip and then from the lateral pressures and displacement as the pile length moves into the region. There is a build up in pore pressure throughout the area of local shear failure. Accompanying this process is a continuing movement of the pile surface through the region. The failure zone close to, but not on, the pile surface associated with this movement produces a somewhat less dense particle arrangement, while movement is still in progress, lowering locally within this failure mechanism, the excess pore water pressure produced by the initial yield. This tends to draw moisture from the surrounding soil to the failure zone and accelerates the yield process. Upon cessation of movement, pore water pressure near the pile surface rises for a time as this region of yield and movement assumes a denser arrangement until general equilibrium exists in the entire region of local shear failure. Dissipation of excess pore water pressure occurs simultaneously at the outer fringes of the region of local shear into the less disturbed general shear region. This process continues, allowing the soil structure to assume a denser arrangement in a consolidation process, the speed of which is a function of the soil structures within the regions of shear failure as well as in the undisturbed soil.

Upon static loading to ultimate bearing capacity and plunge, the same process is, to a lesser degree, repeated. The failure mechanism at the point develops in this case according to the theory of Meyerhof. The

dense soil structure in the immediate vicinity of the pile surface yields and relative movement occurs between soil particles, resulting, during movement, in a less dense soil arrangement. Upon cessation of movement, the soil structure returns to a denser arrangement. As shown in Figure 2.7, the region of large relative movements between soil particles should be much more local for the case of failure due to static loading than for the dynamic failures which take place during driving. This is attributed to the fact that contact between soil particles is much better developed after the excess pore water pressures created during driving have dissipated. Static failure of the soil structure assumes the form of a fracture pattern as opposed to the dynamic flow pattern developed during driving. As commonly observed in practice when a pile is pulled from the soil, failure occurs within the soil rather than directly upon the pile surface. The extensive particle contact developed by flow and pressure along the pile surface results in a higher adhesion at the pile surface than that of the cohesion in the soil a small radial distance from the pile surface.

It is the conclusion of the authors, that location and dimensional extents of static and dynamic zones of failure along the length of the pile are as shown in Figure 2.7. The fracture and flow zone dimensions are based upon comparisons of the magnitudes and dissipation patterns of excess pore water pressures resulting from the respective failures rather than an analytic analysis.

Thus, pore pressures and soil structure combine to produce a response which is an interaction of the two. Both static and dynamic load transfer is accomplished through a soil particle structure which is primarily a function of any unexpelled pore water pressures.

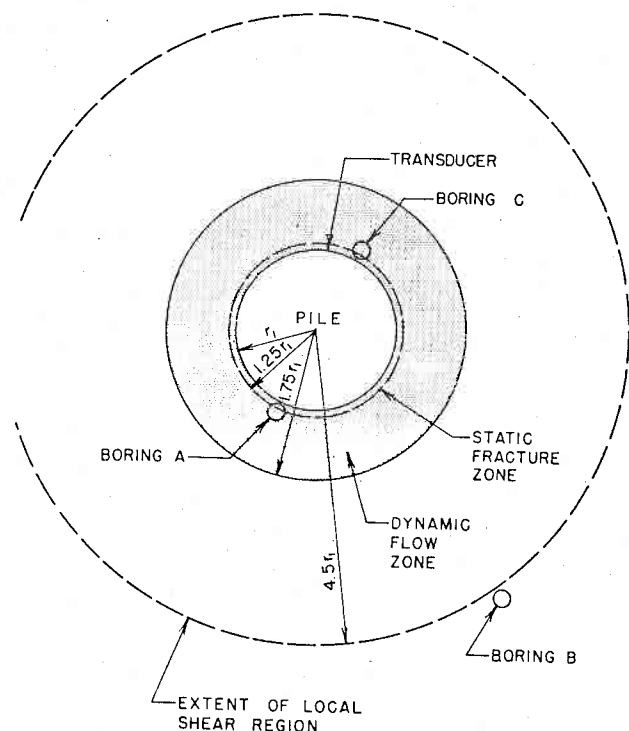


Figure 2.7. Soil failure adjacent to pile.

CHAPTER III

PORE WATER PRESSURE FLUCTUATIONS ASSOCIATED WITH A PILE DRIVEN INTO A SATURATED COHESIVE SOIL

General

One of the most widely observed phenomenon associated with various loadings of saturated cohesive soils is the fluctuation of pore water pressure with load application and time (34). Such has been the case also with the soil loadings associated with pile driving. The disruption of the saturated soil structure around the periphery of the pile results in a change in void ratio and subsequent change in pore water pressure of the relatively incompressible soil water. These changes in pressure then become involved in the already complex mechanism of load response of the pile-soil system. Upon completion of loading, the differential between the pore water pressure in the immediate vicinity of the pile and that of the surrounding soil medium is reduced through a dissipation process. The magnitude and duration of this differential is a function of the magnitude and dimensional extent of soil disturbance, as well as the permeability and diffusivity of the soil.

Several authors have investigated the excess pore water pressures developed during pile driving and sought to correlate the dissipation of these pressures with the load-carrying capacity of the pile (9) (25) (31).

Theory of Reese and Seed

Reese and Seed (25) noted that Terzaghi (34) had applied the equations of heat diffusion to the problem of one dimensional consolidation, and extended the analogy to the radial dissipation of excess hydrostatic pressure from the surface of a pile. The diffusion equation is applicable to this case when expressed in the cylindrical coordinate system:

$$K \left[\frac{\partial^2 u}{\partial r^2} + \frac{1}{r} \frac{\partial u}{\partial r} \right] = \frac{\partial u}{\partial t} \quad (3.1)$$

where: u = excess hydrostatic pressure
 r = radial coordinate
 t = time
 K = diffusivity constant

Without going through the details of the solution, Reese and Seed used the solution for this equation as presented by Carslaw and Jaeger (4):

$$u = \frac{Q}{2\pi} \int_0^\infty e^{-Kv^2 t} \frac{[A] [B]}{J_1^2(vr_1) + Y_1^2(vr_1)} v dv \quad (3.2)$$

where: $A = J_1(vr_1) Y_0(vc) - J_0(vc) Y_1(vr_1)$
 $B = J_1(vr_1) Y_0(vr) - J_0(vr) Y_1(vr_1)$
 u = excess hydrostatic pressure
 Q = strength of instantaneous surface source

K = diffusivity
 t = time
 v = dummy variable
 J_0 = Bessel function of the first kind of order zero
 J_1 = Bessel function of the first kind of order one
 Y_0 = Bessel function of the second kind of order zero
 Y_1 = Bessel function of the second kind of order one

In order to apply this solution, originally obtained for an instantaneous heat surface source acting over the surface $r = c$ at $t = 0$, to the problem of dissipation of excess pore water pressures, Reese and Seed were compelled to assume an instantaneous surface source of strength Q applied at the pile surface. Such an assumption was not illogical when the soil medium into which the pile was driven is assumed to behave as a viscous fluid.

In order to obtain a practical relationship for the highly complex integral presented in the solution of Carslaw and Jaeger without resorting to involved numerical procedures to accomplish the integration, Reese and Seed performed certain mathematical simplifications. Noting that in order for the integral to have significant magnitude, v must be very small for large values of Kt , they obtained approximate evaluations of the involved Bessel functions applicable for the case of large values of time. Such relationships, which are reasonable for the values of time significant in the response of the pile-soil system, are as follows, for small x :

$$\begin{aligned} J_0(x) &\approx 1 \\ J_1(x) &\approx \frac{x}{2} \\ Y_0(x) &\approx \frac{2}{\pi} \ln \frac{x}{2} \\ Y_1(x) &\approx -\frac{2}{\pi x} \end{aligned}$$

where: x = general variable

Substitution of these simplifications into the integral allows the integration:

$$u \approx \frac{Q}{2\pi} \int_0^\infty e^{-Kv^2 t} v dv = \frac{Q}{4\pi Kt} \quad (3.3)$$

It may be noted that this solution is *independent* of the *radius* of the pile. Further, it is assumed that all material exterior to the surface of the pile is of uniform diffusion characteristics. It is also based upon the assumption that the source of excess pore water pressure exists in the immediate area of the pile surface.

Theory of Soderberg

Perhaps the most comprehensive article to be found in the literature concerning the time effects of load response of the pile-soil system has been presented by Soderberg (31). In this article, Soderberg has correlated a numerical solution to the problem of pore water pressure dissipation with the load response of several test piles reported in publications and private communications. Soderberg begins his approach with the basic theory of consolidation, as presented by Terzaghi (34). Thus, the flow of water across a small finite element, bounded by radial dimensions, less the change in volume of water contained in the element, can be expressed as follows:

$$\frac{\partial (dV_w)}{\partial t} = \frac{k r d\theta dr}{\gamma_w} \left(\frac{\partial^2 u}{\partial r^2} + \frac{\partial u}{r \partial r} \right) \quad (3.4)$$

where: dV_w = volume of water contained by the element

k = coefficient of permeability

r = radius

θ = angle

γ_w = unit weight of water

u = hydrostatic excess pressure

The time derivative of the volume of water in the element is:

$$\frac{\partial (dV_w)}{\partial t} = \frac{r d\theta dr}{1 + e} \frac{de}{dt} \quad (3.5)$$

where: e = void ratio of the soil

Soderberg then substitutes $(a_h)(du)$ for de and defines

$$C_h = \frac{k(1+e)}{a_h \gamma_w}$$

and equates the two. He notes that a_h is the horizontal coefficient of compressibility. Thus, the partial differential equation becomes

$$\frac{\partial u}{\partial t} = C_h \left(\frac{\partial^2 u}{\partial r^2} + \frac{\partial u}{r \partial r} \right) \quad (3.6)$$

This solution requires that an average horizontal coefficient of consolidation be assumed over the radial distance disturbed by driving. With this assumption, the above partial differential equation may be solved. Reese and Seed restricted their solution to one assumed initial excess pore pressure source. Soderberg, on the other hand, presents the dissipation curves to be expected according to two analyses of soil disturbances. These alternate analyses were derived from two basic assumptions of the behavior of soil as an engineering material. One assumption is that the soil acts as a perfectly elastic-plastic material. The other is that, at the instant of completion of driving, the soil acts as a viscous substance which will not support tension, i.e., a viscous liquid.

With the two alternate initial excess pore water pressure distributions established, Soderberg duplicates the basic partial differential equation numerically:

$$\begin{aligned} & \frac{U_o - u_o}{h_t} \\ &= C_h \left(\frac{u_2 - 2u_o - u_1}{h_r^2} + \frac{u_2 - u_1}{r 2 h_r} \right) \quad (3.7) \end{aligned}$$

where: U_o = hydrostatic excess pressure at zero time

h_t = chosen time interval

u_o = the hydrostatic excess pressure at time t

h_r = radial space increment referred to by subscripts

If, in this equation, $\frac{C_h h_t}{h_r^2}$ is set at 0.25 for convenience

in computation and plotting and radial distance r is replaced by the numerical nh_r where n refers to the space intervals from the point of consideration to the pile center, the equation reduces to:

$$\begin{aligned} U_o &= u_1 \left(0.25 - \frac{1}{8n} \right) \\ &+ u_2 \left(0.25 + \frac{1}{8n} \right) + 0.5 u_o \quad (3.8) \end{aligned}$$

On the basis of this equation the curves shown in Figure 3.1 as presented by Soderberg may be obtained:

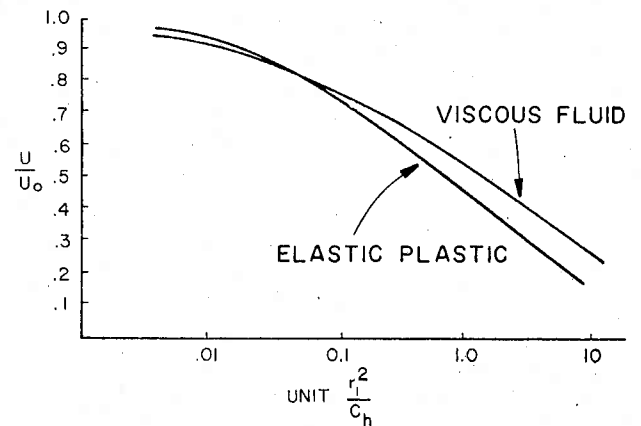


Figure 3.1. Initial pore pressure patterns from Soderberg (31).

As Soderberg has indicated, it is important to note that, while the alternate curves differ with the initial disturbance assumed, since they are both based upon Carslaw and Jaeger's mathematical solutions, they are

a function of $\frac{r_1^2}{4 C_h t}$, where r_1 refers to the radius of the

pile. Thus, the lateral dimension of the pile along with the coefficient of consolidation of the soil determines the time required for pore water pressure dissipation.

Proposed New Theory

The model designed by Reese and Seed does not correspond satisfactorily to the recognized physical origin of the excess pore water pressure as a function of the size of the pile. The numerical model presented by Soderberg, on the other hand, incorporated the pile dimension as well as an explanation of the physical origin of the excess pore water pressure. It is considered to present the better description for long term dissipation patterns. However, it does not recognize the effect of the disruption of the existing soil structure in the region immediately surrounding the pile, which greatly influences initial pore pressure dissipation patterns. On the

contrary, it averages the soil properties of the various states of disturbance over the entire soil medium. It is the intent of the authors at this point to propose a mathematical model which does take into account the radius of the pile and the soil permeability and diffusion characteristics for the states of soil disturbance proposed in Chapter II. Such a model will furnish a better description of initial pore pressure dissipations than the currently available approaches.

Immediately upon the completion of driving, there exists, within a radial distance of 4.5 radii from the pile center, a circumferential region of soil which has undergone local shear failure and displacement. As presented in Chapter II, this disturbance is due to the stresses imposed during driving. Within this region of disturbance, the disruption and displacement of the existing soil structure results in an excess pore water pressure. The region in which the soil has been subjected to general shear failure extends outward from a radial distance of 4.5 radii from the pile center as shown in Figure 2.7. The soil structure within this region of general shear failure has remained essentially unaltered, and it is assumed for analysis that the permeability as well as the pore water pressure of this region remains, at this point, essentially unaltered.

The differential equation describing this process is again, of course, the diffusion equation:

$$K \left[\frac{\partial^2 u}{\partial r^2} + \frac{1}{r} \frac{\partial u}{\partial r} \right] = \frac{\partial u}{\partial t} \quad (3.9)$$

where: u = excess hydrostatic pressure

K = diffusivity constant

The solution of this equation has been obtained by Carslaw and Jaeger (4) for the case of heat diffusion. The analysis is rather involved and will not be recapitulated here. In general terms, it involves applying a Laplace transformation to the partial differential equation for diffusion in order to obtain an equation in terms of total derivatives. Then, simultaneous differential equations can be written for the region $0 < r < a$ in which an excess hydrostatic pore water pressure (or initial temperature, in the original equation of Carslaw and Jaeger) exists, as well as for the outer regions $r > a$, where it is zero.

Utilizing the existing boundary conditions, a solution for these equations may be obtained. By use of an Inversion Theorem, as presented by Carslaw and Jaeger, this solution may be converted back into terms of the original physical parameters. The equations obtained, still in terms of heat transfer, are:

$$v_1 = \frac{4 V K_1 K_2 k_2}{\pi^2 a} \int_0^\infty e^{-k_1 u^2 t} \frac{J_0(ur) J_1(ua)}{u^2 [\phi^2(u) + \Psi^2(u)]} du \quad (3.10)$$

$$v_2 = \frac{2 V K_1 k_2^{1/2}}{\pi} \int_0^\infty e^{-k_1 u^2 t}$$

$$\frac{J_1(ua) [J_0(kur)\phi(u) - Y_0(kur)\Psi(u)]}{u [\phi^2(u) + \Psi^2(u)]} du \quad (3.11)$$

where: the subscripted symbols are diffusion properties of the two regions

$$k = \sqrt{\frac{k_1}{k_2}}$$

$$\Psi(u) = K_1 K_2^{1/2} J_1(au) J_0(kau) - K_2 k_1^{1/2} J_0(au) J_1(kau)$$

$$\phi(u) = K_1 K_2^{1/2} J_1(au) Y_0(kau) - K_2 k_1^{1/2} J_0(au) Y_1(kau)$$

These expressions are obviously too complicated to illustrate the physical significance of the various parameters. Following the same procedure as Seed and Reese, however, one may obtain a more simplified solution of these equations for the relatively large values of t of interest in this study. Then for small values of u in the expression, the approximations, with χ as the general variable, are:

$$J_0(x) \approx 1 \quad J_1(x) \approx \frac{x}{2}$$

$$Y_0(x) \approx \frac{2}{\pi} \ln \frac{x}{2} \quad Y_1(x) \approx -\frac{2}{\pi x}$$

Substituting these approximations into v_1 which corresponds to the excess pore pressure within the local shear region, neglecting higher orders of small quantities, and simplifying the expression, the integral becomes:

$$v_1 \approx \frac{V K_1 a^2}{2 K_2} \int_0^\infty e^{-k_1 u^2 t} u du \quad (3.12)$$

which may be integrated to obtain:

$$v_1 \approx \frac{V K_1 a^2}{4 K_2 k_1 t} \quad (3.13)$$

or in terms of previous expressions:

$$u_1 \approx \frac{Q K_1 a^2}{4 K_2 k_1 t} \quad (3.14)$$

where: Q = excess pore water pressure in region of local shear failure

u_1 = excess pore water pressure in soil adjacent to the pile surface

K_1 = permeability of region of local shear failure

K_2 = permeability of region of general shear failure

k_1 = diffusivity of region of local shear failure

t = time

a^2 = radial dimension of region of local shear failure

An examination of this final expression reveals that it involves the permeability and diffusion properties of the soil in the regions of disturbance and the radial extent of local shear failure. This is in itself a function of the lateral dimensions of the pile as well as the plastic strength of the soil, as demonstrated in Chapter II. As previously indicated, it is considered that the mathematical model presented by Soderberg will adequately describe long term pressure dissipations. The dissipation

pattern described by this linear mathematical model does approach the semi-logarithmic pattern presented by Soderberg with time as high initial pressures decay and dissipation becomes a conventional consolidation process. The linear pattern serves to slow down initial pore pressure dissipations in order to describe the influence of change in soil properties due to disturbance in the region undergoing local shear failure. Such effects are most noticeable in cases involving large diameter piles since the region undergoing local shear failure becomes progressively more significant with increase in pile diameter.

Another area of interest in pore water pressure measurements concerns the fluctuations associated with the deformation of the soil structure during static loading of the pile after the high pore pressures resulting from driving have dissipated. It is logical to expect the pore pressures within the dense soil particle arrangement adjacent to the pile surface to rise somewhat with increasing load on the pile as the soil strains elastically in supporting the applied load. If, however, the pile is loaded to its ultimate bearing capacity and actually

plunges, the resulting downward movement could be expected to produce momentarily a less dense arrangement of particles and particle complexes, as they move relative to one another during shear strain. Following cessation of shear strain, the particles can settle into an interlocking pattern to form a denser arrangement than could be achieved during movement of the pile. Such readjustment of the soil particles would be reflected by a slight increase in pore pressures during loading to ultimate capacity, a lowering of pressures while movement was actually taking place, and, finally, a rise again in pore pressures once the load was removed and downward movement of the pile ceased. This final rise in pore pressures would bring them to levels above which they stood prior to loading, providing a denser arrangement of soil particles resulted from their relative movements. According to the model of soil failure presented in Chapter II for static loading, however, the magnitude and duration of excess pore pressures resulting from such slow failures should be less significant than those observed for dynamic, or sudden failures, since a much smaller region of soil is subjected to disturbance.

CHAPTER IV

STATIC AND DYNAMIC RESPONSE TO LOADING OF THE PILE-SOIL SYSTEM

General

Investigations of the mechanical response of foundations subjected to dynamic loading have long attracted the attention of researchers (1) (23) (26) (34) (39). Several theoretical approaches to the specific problem of loadings associated with pile driving have been presented since it was first recognized that the dynamic response of the pile took the form of a longitudinal vibration described by the one dimensional wave equation (7) (13) (17) (29) (39). The theory pertaining to this response has been used in the estimation of the ultimate bearing capacity of the pile by means of observations taken at the time of driving (8) (11). Interest in the dynamic response of piling during driving has been extended to problems concerning cracking of long concrete piles due to tensile forces (13) (17).

A computer program developed at Texas A&M University utilizes the discrete element numerical approach first proposed by Smith (30) in order to describe the dynamic response of the pile to a hammer blow. Such an approach facilitates detailed description of the forces acting on a given pile segment. The interaction of all pile segments in the system forms the response of the entire system. The interaction can be analyzed on a high speed digital computer using Smith's finite time interval technique (28). Field tests have substantiated the accuracy with which this mathematical model and computer program duplicate the mechanical elements of the pile-soil system (15) (27). The initial research is being extended, by application of the computer program, to estimation of the ultimate bearing capacity of the pile, as a function of the dynamic response of the pile-soil system during driving (16).

Recent advances in the dynamic testing of soils now permit a more diversified approach to the problem of

dynamic soil response (6) (24). Ultimately, this may lead to a better correlation of the dynamic response of the pile-soil system to the ultimate load bearing capacity of the system.

Nature of Dynamic Response

The dynamic response of the pile-soil system develops in accordance with the failure mechanism presented in Figure 2.7. The sequence of events involved in soil failure adjacent to an element of the pile is as follows:

1. Initially, the soil deflects elastically until its full shear strength is exceeded.
2. The soil yields plastically.
3. Finally, the soil rebounds elastically to its permanent set.

Previous studies have suggested that the magnitude of the dynamic soil deflection is of the order of one tenth of an inch (30). Such values are based upon observations made during static load tests (7). It has been suggested from the previous studies that the energy required to deflect the soil elastically to the indicated extent can be expressed by considering the soil as thick plates upon elastic foundations (10) (3) (12) (38). Then, that part of the energy applied to the pile which does not produce permanent set, is consumed in causing the elastic deflection of the soil. The failure mechanism discussed previously includes relatively small radial dimensions of soil. These dimensions dictate a much smaller magnitude of elastic deformation of the order of one hundredth of an inch, in order to mobilize the full shear strength of the soil. Laboratory tests upon model piles (24) indicate that this is the case. It is proposed in this study that these smaller elastic yields

are applicable for the time rates of dynamic loading encountered in driving, and that practically all energy imparted to the pile by the hammer, which is not utilized in producing permanent set, is dissipated from the area of loading in the form of a compression or transverse wave (1) (10) (19) (24).

The total dynamic response of a saturated-cohesive soil as it undergoes plastic yield, is composed of two components; a static friction force and viscous damping force. The friction force is independent of the rate of loading and is an indication of the effort required to overcome the soil friction to produce relative displacements. The magnitude of the viscous force is proportional to the rate of loading. This force results from relative displacements across large regions of soil as shown in the dynamic flow zone of Figure 2.7, as individual soil particles, soil particle complexes, and pore water are caused to flow in a zone of failure.

Nature of Static Response

Static loads are applied to piles so slowly that the viscous component of response is negligible. The ultimate bearing capacity, as determined by static loading

of friction piles is, therefore, a function of the soil friction. The analysis of factors influencing the static load response is in effect an analysis of factors influencing soil particle contacts. As indicated in Chapter II, for the case of friction piles driven into saturated cohesive soil, the most important factor influencing the development of soil particle contacts associated with a denser soil structure is the excess pore water pressure. The ultimate load bearing capacity, which a friction pile will develop, is usually measured by load test only after excess pore water pressures have dissipated and the soil has attained its final consolidated structure. The load bearing capacity attained by a friction pile then becomes a function of the shear strength of the disturbed and reconsolidated soil along the length of the pile and of any point load developed.

The slow rates of load application during static load tests result in a less extensive shear failure mechanism than that developed by dynamic load application during driving. The dimensional extent of the failure mechanism developed during static loading closely approximates that presented by Meyerhof as shown in Figure 2.4.

CHAPTER V

PILE FABRICATION AND INSTRUMENTATION

The Pile and Its Fabrication

The pile was a steel pipe 53 ft. long, 16 in. in diameter and $\frac{3}{8}$ in. wall thickness (see Figure 5.1). Driving was accomplished by a Standard Delmag D-12 diesel hammer without a cushion block (see Figure 5.2). Driving of the test pile was accomplished by a contractor serving the Texas Highway Department, District 20. The pile used served as a test pile for an overpass project in Beaumont, Texas. Waterproof bulkheads of $\frac{3}{8}$ in. steel plate were provided at the top and approximately $1\frac{1}{2}$ in. inside the bearing plate at the bottom of the pile. The bottom bearing plate was formed of $\frac{7}{8}$ in. thick steel plate. A $\frac{3}{16}$ in. thick open end segment, approximately one foot in length, was welded to the top of the test pile in order to adapt it to the driving cap of the hammer (see Figure 5.3).

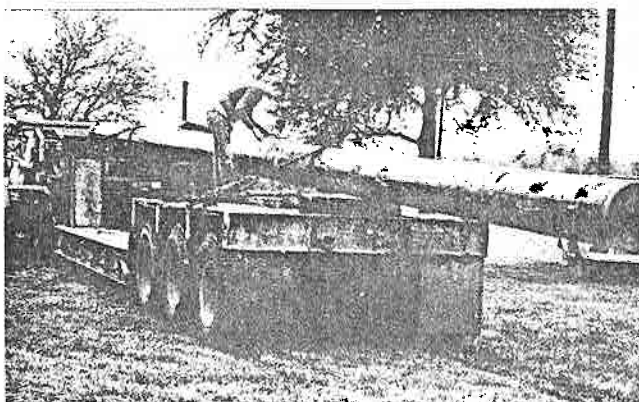


Figure 5.1 Test pile.



Figure 5.2. Diesel hammer.



Figure 5.3. Welding open end segment.

ment installations and the pile wall in order to reduce both stress concentrations and fatigue during the shock loads associated with driving.

In order to accomplish the basic objectives of this research, the instrumentation was necessarily subjected to a more severe environment than would have been the case under conditions arbitrarily chosen to protect the instrumentation from damage. Of primary concern in

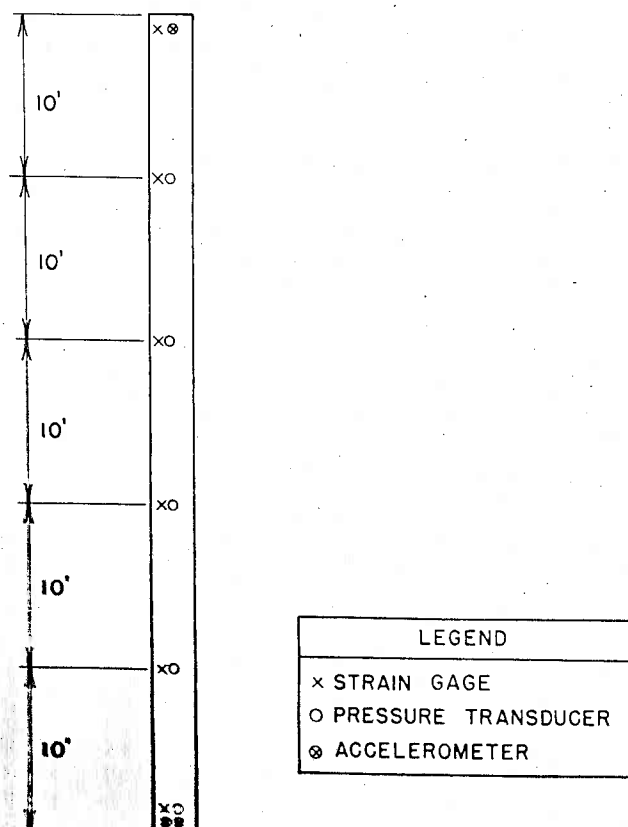


Figure 5.4. Instrument location.

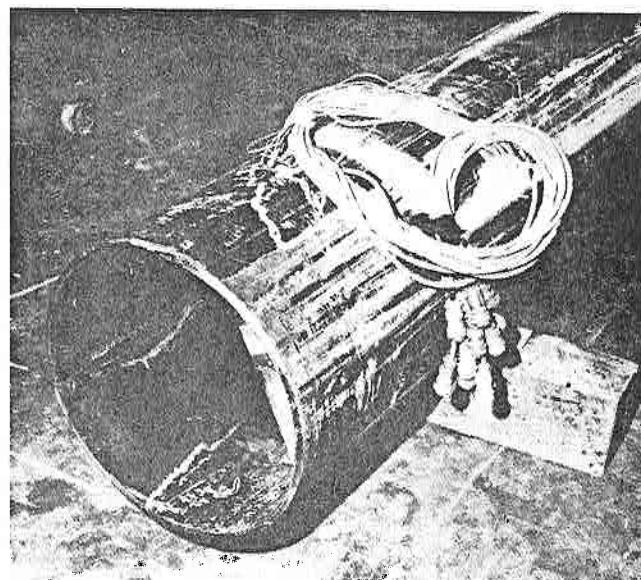


Figure 5.5. Instrument leads.

the installation of the instrumentation was the rather severe shock and acceleration to which all instruments and wiring were subjected. All of the conditions normally associated with pile driving were present and intensified by the steel to steel contact between the hammer and pile because of the elimination of the cushion block. Another consideration in the instrumentation and wiring installation was the moisture environment to be expected and the length of time which the instruments would be required to operate. Most of the length of the pile was under the water table and the top of the pile could be expected to be subjected to rainfall and extremely wet conditions during soil sampling. Furthermore, condensation of moisture within the interior of the pile could be expected. Difficulties were encountered in strain gage placement which required a controlled environment

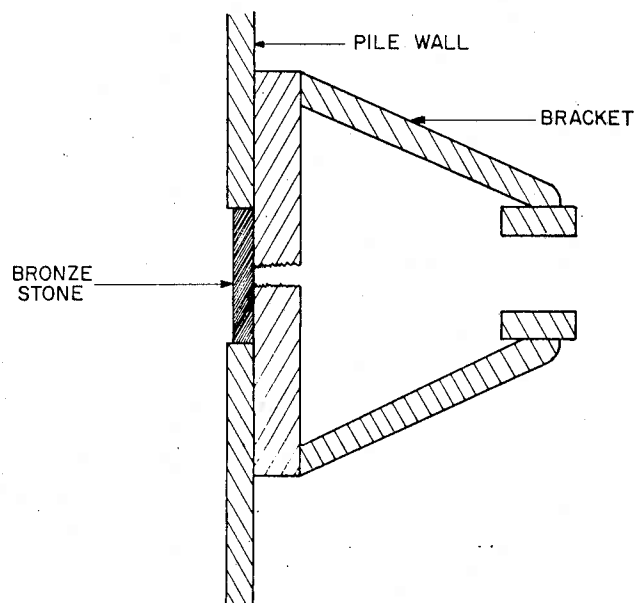


Figure 5.6. Pressure transducer installation.

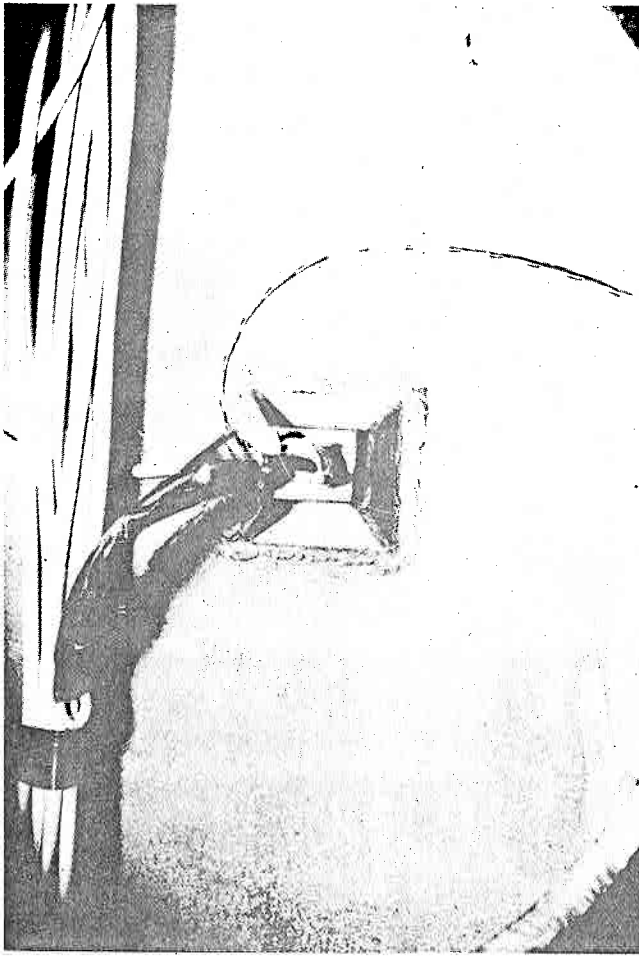


Figure 5.7 Strain gage leads and pressure transducer installation.

for the curing of the Epoxy Cement C-2 with which the gages were attached to the pile. Also, the steel of the pipe contained small flaws which interfered with strain gage placement.

Instrumentation

Excess pore water pressure measurements were obtained with Consolidated Electrodynamics Corporation Type 4-326 pressure transducers. Important design features included corrosion resistant housings, 0-100 psi gage ranges, and ability to withstand a 1000 g half sine wave pulse for the duration of one millisecond without damage. The pressure transducers were mated to the pile wall as shown in Figure 5.6. The transducer support was necessary in order to protect the instrument from breakage through bending during driving. The porous bronze plates prevented the entry of foreign material into the transducer diaphragm chamber. In order to lower the response time of the instrument, the pressure transducer was filled with water before the protective porous bronze plates were fastened in position with epoxy. The pile was transported with the porous bronze plates oriented upward and covered to preclude loss of water from the transducer through seepage and evaporation. Upon arrival at the test site the installation was checked and the bronze plates moistened again as an added precaution. A thin layer of clay was

applied to the porous bronze plates to minimize loss of contained water by seepage, as the pile was hoisted to a vertical position and driven. These precautions resulted in a lowering of the response time of the instruments to the extent that pressure measurements recorded, other than those due to shock waves during driving, were considered to be those existing in the soil.

Stresses in the pile were measured by Micro-Measurements C6-121-R2TC strain gage rosettes that were cemented to the pile wall in pairs on opposite sides of the wall. Epoxy cement was used. The four active gages were wired in a full bridge to compensate for lateral deflection and temperature differentials (see Figures 5.7 and 5.8).

Accelerometers were installed at the top and bottom of the pile in order to measure the acceleration of these particular locations. The instruments were centrally mounted on 4 in. I-beams placed diametrically across the pipe and continuously welded at each end to produce a stiff joint (see Figure 5.8). This arrangement was designed to produce a very high natural frequency of the accelerometer mounting itself which could not be detected in the accelerometer readings. Two Statham accelerometers were mounted at the bottom of the pile with respective ranges of 0-100 g's and 0-250 g's. An Endevco 2211 C accelerometer was placed at the pile head in lieu of the intended Statham instrument when

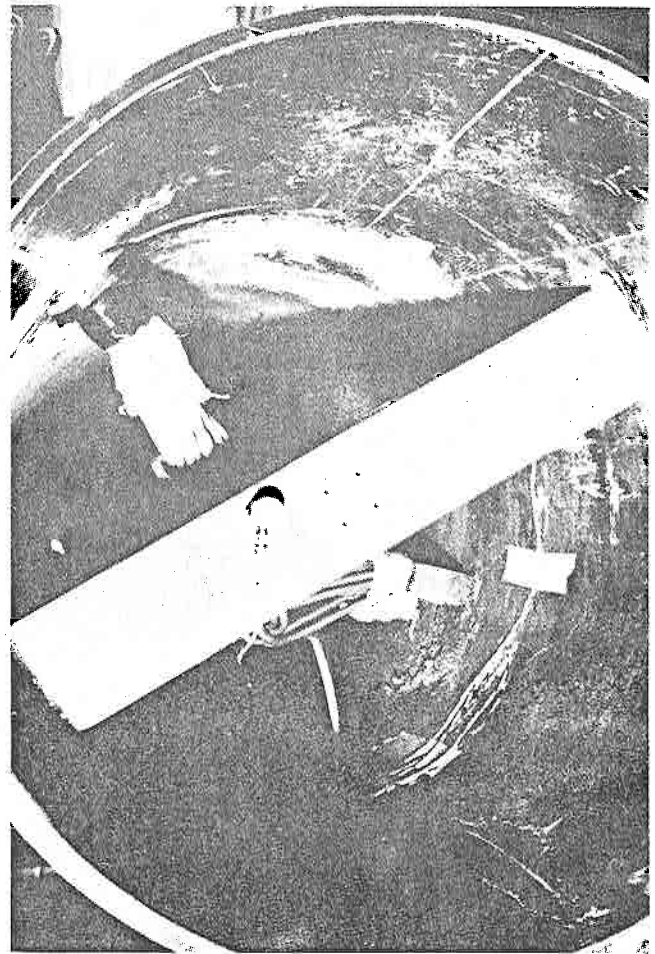


Figure 5.8. Accelerometer installation.

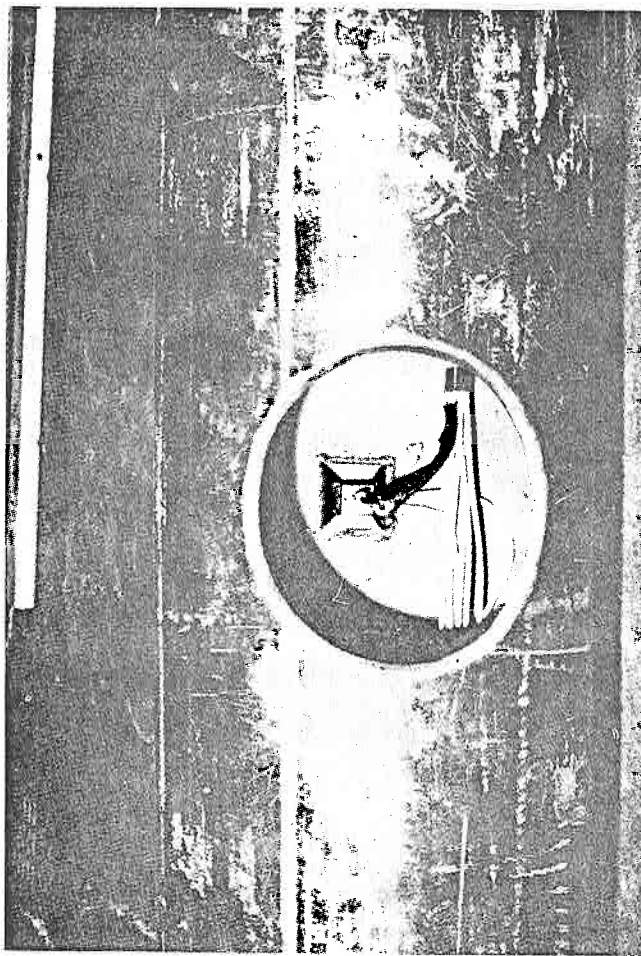


Figure 5.9. Access port.

the original instrument did not arrive in time for the scheduled test.

Instrumentation was installed in the pile, as shown in Figure 5.9, through access ports which were later welded back in place and from the ends of the pile segments before they were joined and the ends of the pile sealed. The various types of instruments were arranged at locations around the pile wall as shown in Figure 5.10 in order to provide enough clearance for leads and facilitate installation. Asbestos wrapping was used to protect lead cables as the pile was welded together.

All instruments were connected to monitoring devices by means of Belden 8404 cable. Exceptions were required only in the case of the pressure transducers where the small size of the mating cable connectors supplied with the instrument required use of Belden 8434-

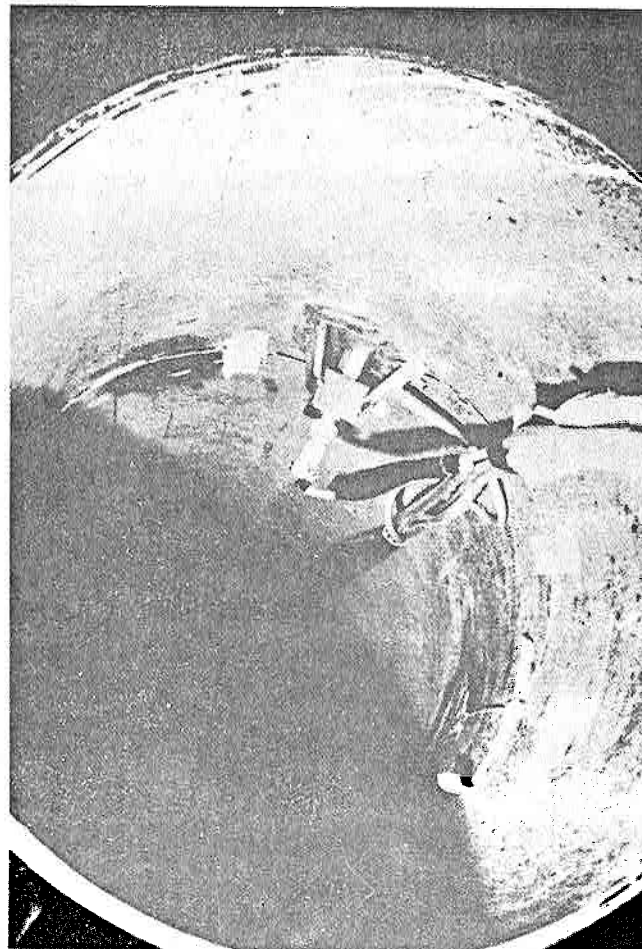


Figure 5.10. Location of instruments around pile wall.

100 leads which were then spliced to the standard Belden 8404 cable. All electrical connections were waterproofed with Gagecoat 5 prior to sealing of the pile to protect them against moisture inside the pile.

Pile instruments were monitored during driving and subsequent static load test by use of a Honeywell 1508 Visicorder oscillograph and Honeywell 119 Carrier Amplifier system. Pore water pressures were monitored by means of a Budd digital strain indicator after driving. This instrument was used also to monitor selected pressure transducers during static load tests in order to obtain more sensitive readings than possible with automatic recording equipment. The use of a digital indicator was possible during static load tests since the time rate of load application and subsequent pore pressure responses were slow enough to allow balancing and reading of the instrument.

CHAPTER VI

LABORATORY AND FIELD SOIL TEST AND SAMPLE PROCEDURES

Soil Profile and Identification Data

The field test site was located on the south side of the City of Beaumont, Texas. A soil profile of the study area is shown in Figure 6.1 along with soil identification

data. The material of prime interest in the study of soil disturbance was the highly plastic clay occurring 35 ft. below the surface. This was due to the fact that the fundamental disturbances were expected to be masked in the shallow surface strata. The highly complex trans-

DEPTH (FT)	SOIL SYMBOL	SAMPLE	DESCRIPTION OF STRATUM	BLOWS/FT.	UNIT DRY WT. LB/CU FT.	PLASTIC LIMIT	PLASTIC INDEX	LIQUID LIMIT	MOISTURE CONTENT %	UNCONFINED SHEAR STR. (PSF)
			FILL ORGANIC CLAY							
			STIFF TAN & GREY SILTY CLAY WITH CALCAREOUS NODULES	98.8	22	34	56	24.5	1750	
10			TAN & GREY SILTY CLAY, SOME SAND	96.3	18	20	38	26.6	1710	
20			SOFT TAN & GREY SILTY SANDY CLAY	107.5	20	22	42	20.8	2740	
			SOFT, SANDY, SILTY, CLAY	101.1	23	12	35	23.6	1490	
30			GREY SAND	40						
				73.3	30	37	67	51.3	2240	
40			FIRM TO STIFF DARK BLUE CLAY WITH SOME SHELLS	68.6	40	42	82	56.5	2215	
				65.4	39	66	105	53.8	2910	
50										
60										





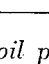
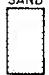

LEGEND			
TYPE OF SAMPLE		SOIL SYMBOL	
	CORE BARREL	 CLAY	 SILT
	DENISON BARREL	 LOW PLASTICITY	 SAND
		 HIGH PLASTICITY	

Figure 6.1. Soil profile.

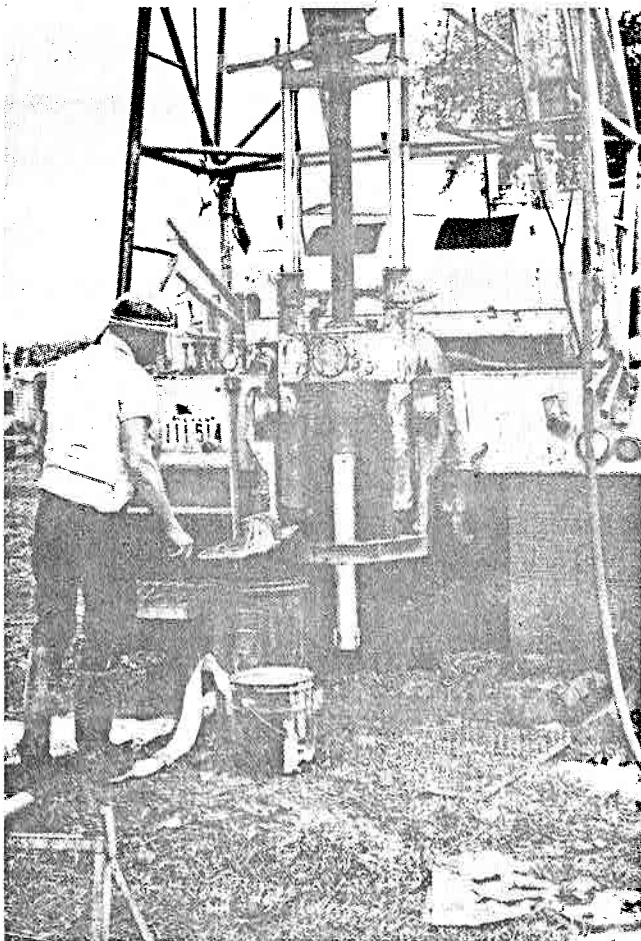


Figure 6.2. Drill rig.



Figure 6.3. Performing vane shear test at field site.

verse loadings imposed upon the soil at these shallow depths during driving would logically result in an erratic pattern of soil disturbances.

Field Sampling Procedures

The soil sampling techniques and test procedures used were designed to measure the soil properties important to the load response of the pile-soil system with the least disturbance to the system possible. In order to accomplish these objectives, it was necessary to obtain soil samples under various states of disturbance and, in the case of the region subjected to local shear failure, before and after pore water pressure dissipation. Of primary concern in planning the soil sampling was the effect of such sampling upon the excess pore water pressures. It was determined prior to driving that careful location of soil borings would minimize such effects. This was verified by continuous pore pressure observations during drilling and sampling.

Soil samples used in this research were recovered with standard thin walled Shelby-tube samplers from borings made with the mobile drilling rig of District 20, Texas Highway Department (see Figure 6.2). As previously indicated, the number and location of borings were chosen to yield the maximum amount of soil information consistent with the least possible disturbance of excess

pore water pressure dissipation. With these considerations in mind, it was decided to make four separate borings. One boring was made before the pile was driven at a distance of approximately 20 ft. from the planned pile location. This boring (boring-D) yielded soil samples of the material in its natural condition. Prior soil exploration performed by the Texas Highway Department indicated that soil conditions in the vicinity were uniform enough to allow use of samples at this distance to determine soil properties in the natural state in the immediate area of the pile. Drilling at this distance left the soil in the future pile location undisturbed prior to driving. The next soil borings were performed immediately upon completion of pile driving. One boring was made very close to the pile surface, approximately 170° radially from the pore pressure transducer locations. The other boring was 2.5 ft. from the pile surface along a radius approximately 30° radially from the previous boring, or 160° from the pressure transducer locations (borings A and B, Figure 2.7). These borings were intended to sample the soil in its initial disturbed condition prior to excess pore pressure dissipation in regions of local shear failure and general shear failure. A final soil boring was made immediately adjacent to the pile surface upon completion of excess pore water pressure dissipation and after all pile load tests had been accomplished 33 days after driving. This boring was made approximately 30° radially from the pore pressure transducer location (boring C, Figure 2.7), and was made in order to obtain soil samples from which changes in soil properties due to pore water pressure dissipation could be measured.

Laboratory Test Procedures

The soil test program consisted of a series of conventional soil tests and newly developed dynamic soil tests, all of which were correlated with miniature vane shear tests performed at the time of sampling. Miniature vane shear tests were performed on soil samples immediately upon their removal from the boring by personnel of the Texas A&M University Soils Laboratory (see Figure 6.3). This procedure was adopted in order to have a measurement of soil shear strength as near as possible to that which existed at the time of driving. By performing vane shear tests on soil samples prior to tests in the laboratory, properties as measured in the laboratory could be better related to field conditions. Miniature vane shear tests were performed on soils at the time of laboratory extrusion from the samplers in the cases of samples without time dependent soil properties. With the exception of this procedure, all conventional soil tests were performed according to currently accepted practice.

Dynamic soil tests were performed according to techniques and procedures recently developed at Texas A&M University. The test procedures used for determination of elastic soil deflection under dynamic load were developed by Raba at Texas A&M University and are described in detail in reference 24. It is considered that this particular dynamic test best duplicates field response of soil acting in friction along a pile surface in that the test effectively reproduces, on a reduced scale, the soil disturbance and mode of failure in the region of local shear failure immediately adjacent to the pile surface.

CHAPTER VII

OBSERVATIONS OF SOIL DISTURBANCES

Pore Pressure Measurements Related to Soil Disturbance

The field observation of soil disturbance can be approached in two ways: through indirect observation by means of pore pressure measurements cor-

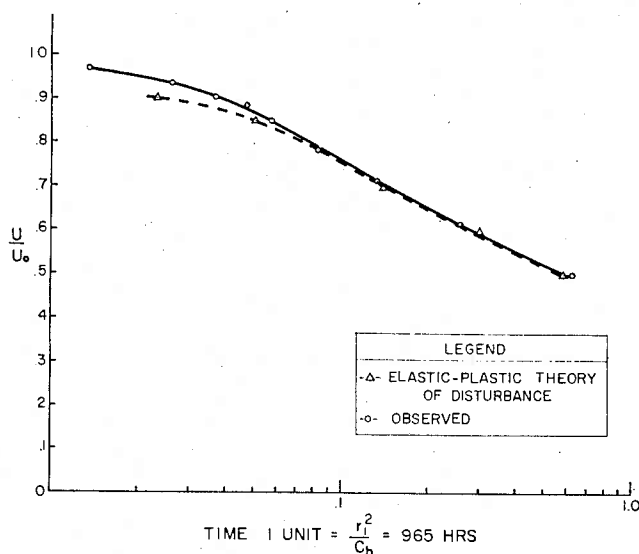


Figure 7.1. Initial pore pressure dissipation—50' depth.

related with a theoretical prediction of this particular response according to assumed modes of deformation; or, through direct observation by means of tests and measurements of soil samples obtained at various radial distances from the pile. As shown in Figure 7.1, the excess pore water dissipation, noted in field measurements, corresponds well with those to be expected according to the ideally elastic-plastic concept of disturbance, as presented by Soderberg. The consolidation characteristics used in this comparison were those determined for soil failed in local shear. It should be noted that this method of observation permits an analytic determination of the extent of local shear failure, since this region corresponds to the region of plastic yield according to the theory of Nadai as applied to soils by Soderberg and presented in Figure 2.2.

Soil Property Measurements Related to Soil Disturbance

In general, it will be shown that results of the soil property measurements support the theoretical predictions of soil disturbances, as presented in Chapter II. The results of the tests for soil shear strengths, by means of miniature vane shear procedure, are presented in Figure 7.2 and Table A-1, Appendix A. As shown by the lines connecting strengths of undisturbed soil (boring D) and soil failed in local shear (boring A), the

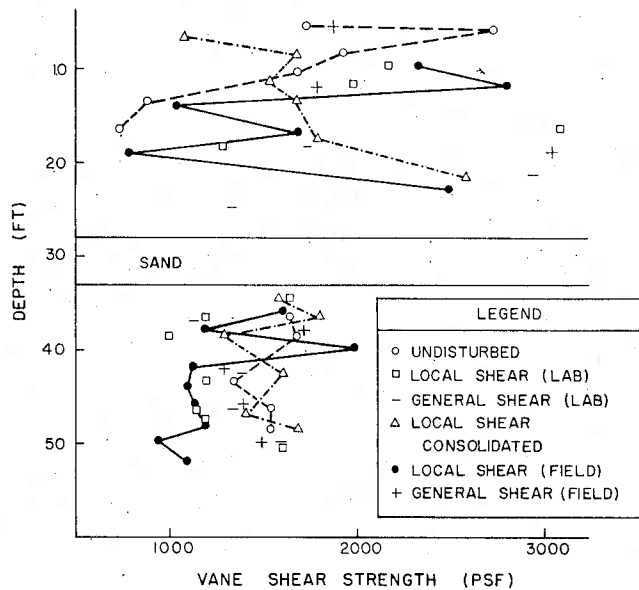


Figure 7.2. Vane shear strengths.

dynamic loading of the shallow strata during driving resulted in a more erratic pattern of soil shear strengths than that which existed prior to driving. At depths of about 10 feet, it may be noted that the tendency was for the soil to increase in shear strength in the zone of local shear. On the other hand, patterns of vane shear strengths determined for the materials underlying the sand stratum indicate definite patterns of changes in soil shear strength as a function of soil disturbance and reconsolidation. Local shear values are less than undisturbed, and local shear consolidated values have increased to closer agreement with undisturbed values.

Values of shear strength determined in the field for soil subjected to local shear failure are generally lower

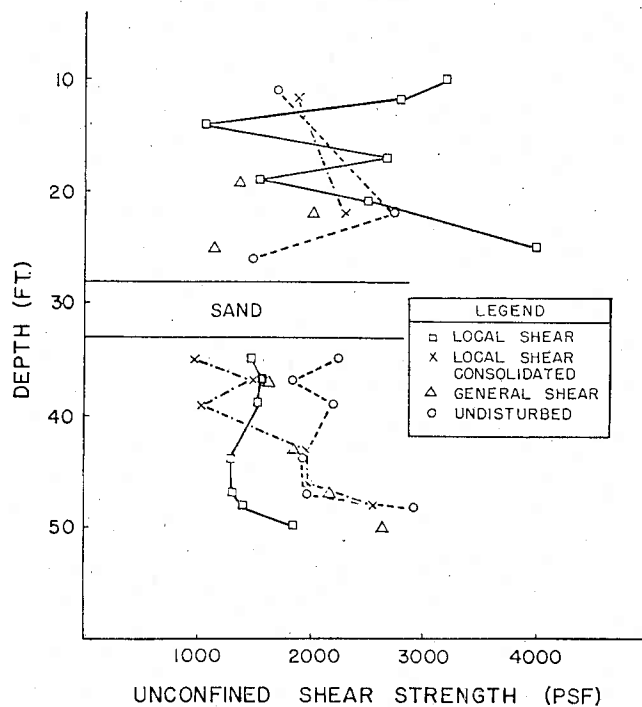


Figure 7.3. Unconfined shear strengths.

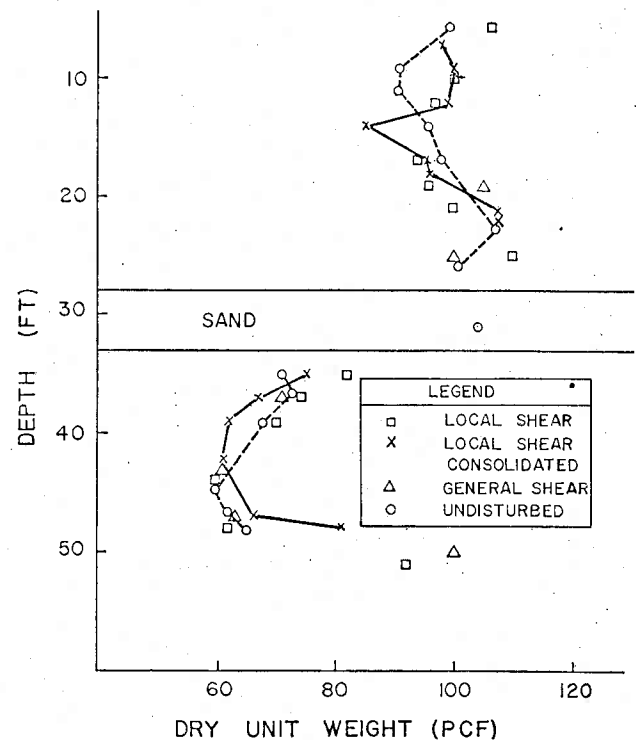


Figure 7.4. Dry unit weights.

than corresponding values of undisturbed soil. These respective values are connected by lines to facilitate comparison. The only erratic plots of vane shear strengths of soil failed in local shear occur at a depth of about 40 ft. At depths greater than 40 ft. an increase in shear strength is noted by the dot-dash line connecting values obtained after the soil failed in local shear consolidates with dissipation of excess pore water pressures.

The results show that soil subjected to general shear (boring B) is not altered greatly in shear strength from

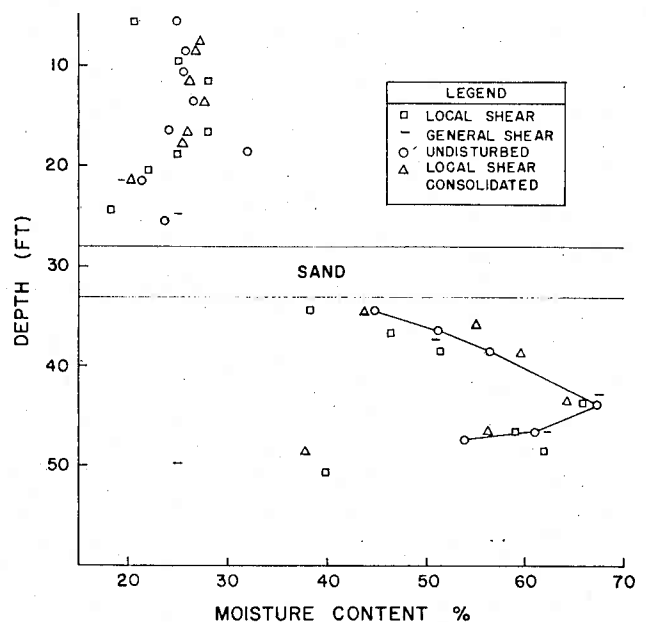


Figure 7.5. Moisture contents.

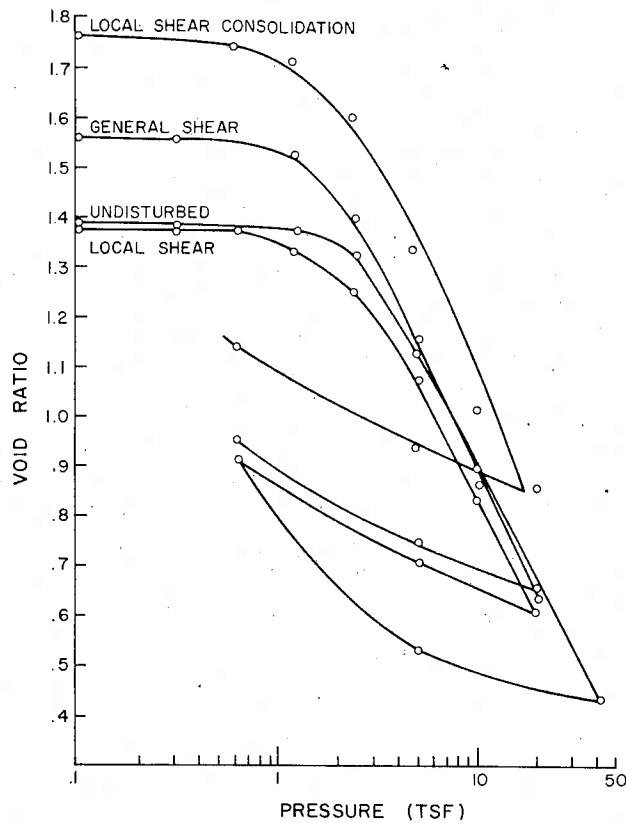


Figure 7.6. Consolidation curves—40' depth.

the undisturbed state. Changes due to time involved in transportation of samples to laboratory facilities are indicated in soil subjected to local and general shear failure. These effects are more pronounced in the case of material failed in local shear.

Values obtained by unconfined shear strength tests are presented in Figure 7.3 and Table A-2, Appendix A. As was the case in vane shear determinations, an erratic pattern of shear strengths in shallow strata developed for the case of local shear. Values obtained for soil subjected to local shear failure are connected by lines to facilitate comparison with similar values determined for undisturbed soil. Unconfined shear strength determinations were required for soil in all clay strata in order to obtain the distribution of the dynamic load response during driving as presented in Chapter IX.

Data from samples taken below the 40 ft. level indicate patterns of the same fluctuations in shear strength with disturbance and reconsolidation as those determined for vane shear strength measurements. The results show a loss in shear strength in the soil from that of undisturbed samples when subjected to local shear failure. With the exception of strata just below the sand, an increase in shear strength is noted in similar soil stratum after reconsolidation from the dot-dash line connecting values determined for the soil in this state. This increase results in a shear strength of approximately the same value as that for undisturbed soil.

Dry unit weights are presented in Figure 7.4 and Table A-3, Appendix A. Soil subjected to local shear failure has a unit dry weight which is about the same as

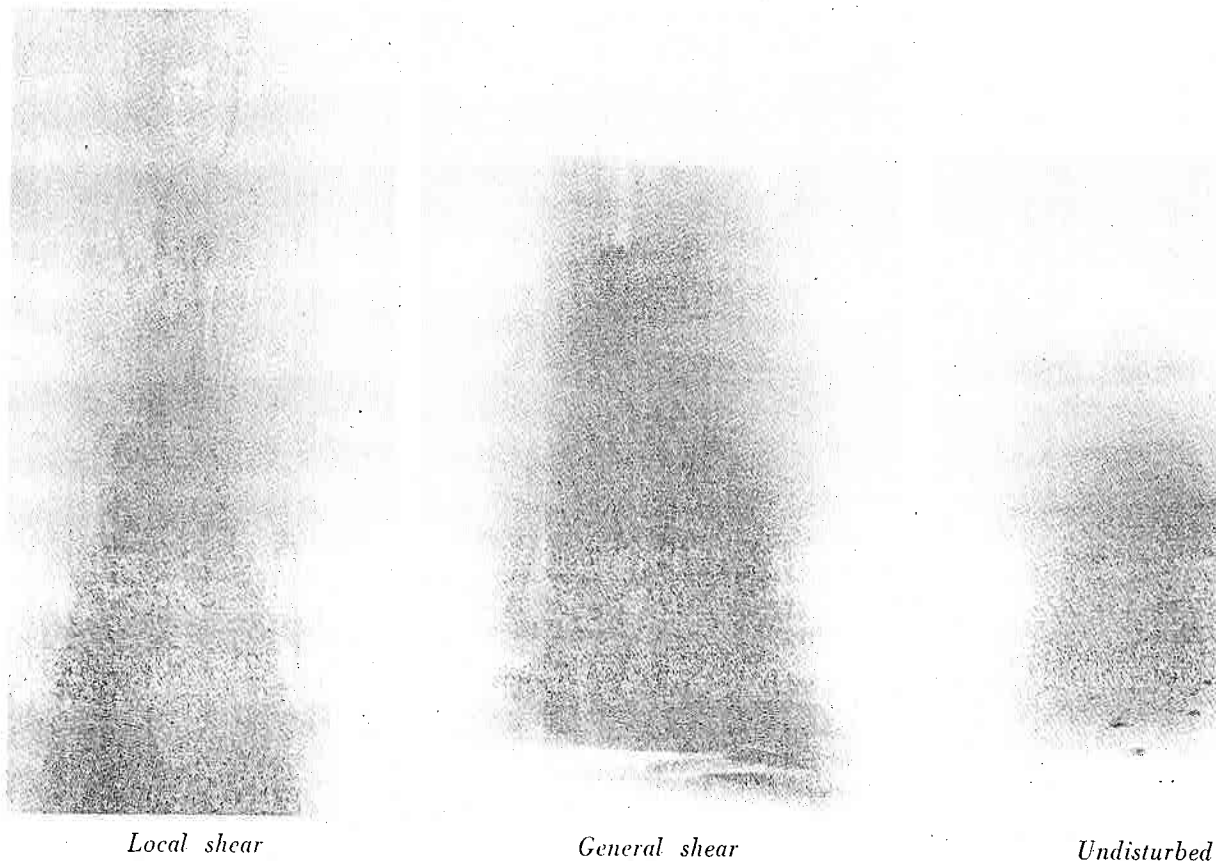
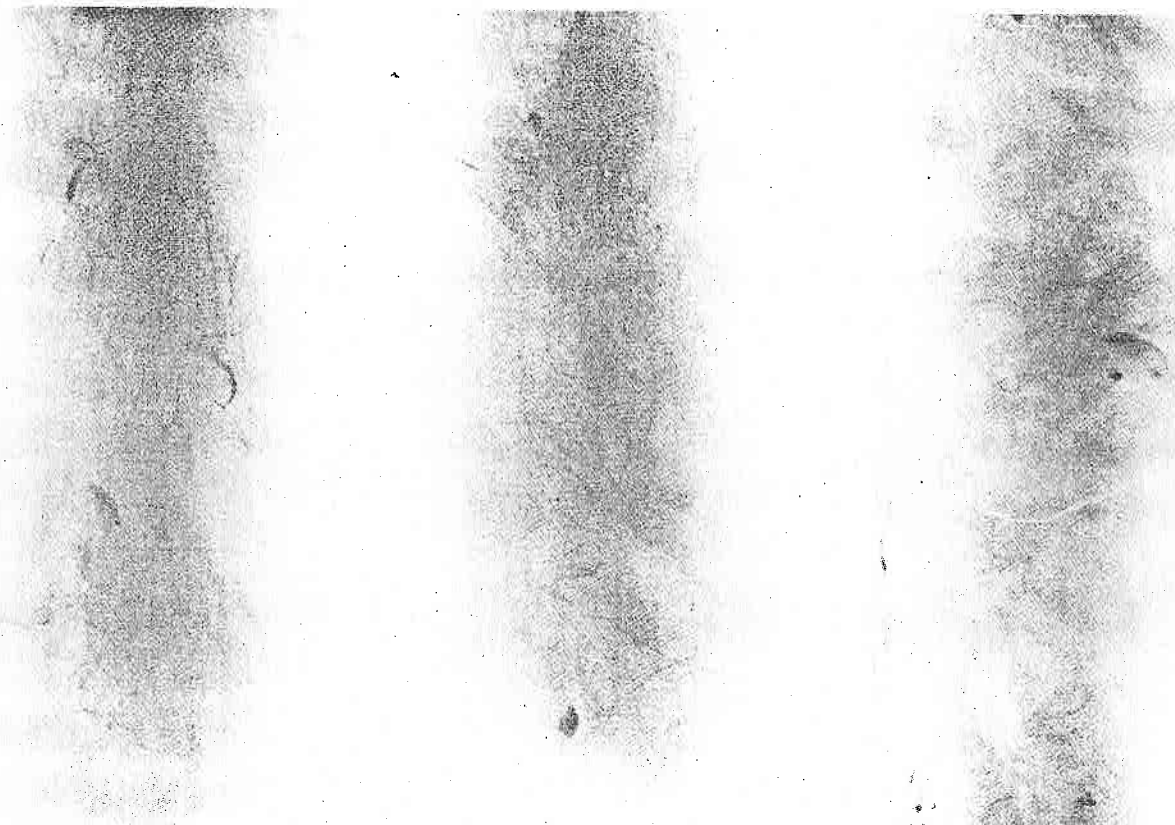


Figure 7.7. Radiogram—40' depth.



Local shear

General shear

Undisturbed

Figure 7.8. Radiogram—15' depth.

that of undisturbed soil. Exceptions may be noted by comparing traces of lines connecting values obtained for these respective soil conditions in shallow strata and the stratum just below the sand in which erratic values of other properties have been noted. A difference does exist between dry unit weights of soil disturbed by local shear failure as determined before and after consolidation in deep material such as at the 49 ft. level. The variation in this property at this depth indicates that large pore water pressure changes may have occurred. Comparison of values obtained at the same time lapse in shallow depths, such as those at 10 ft. where pore pressures were small, indicate very little change in this property.

Moisture contents are presented in Figure 7.5 and Table A-4, Appendix A. These values show very little variation with different states of soil disturbance in shallow strata. It is difficult to make comparisons at greater depths due to the large fluctuations of values even in undisturbed soil, as indicated by the line connecting these values. It is considered that the values obtained at depths of 45 ft. and lower indicate the variation to be expected with disturbance.

Consolidation curves for samples from the different regions of disturbance are presented in Figure 7.6. Since slight variations in depth of sampling may produce large differences in void ratio of the sample, it is considered that the most valuable indications may be obtained from the shape of these curves rather than from direct void ratio-pressure relationships. The curves developed for the undisturbed soil and that subjected to general shear

failure indicate a material with a well developed natural structure, while the curve developed for the soil undergoing local shear failure indicates a remolded condition. The local shear curve is flatter and displaced to the left of the undisturbed curve.

Observation of Soil Structure Disturbance by Means of X-ray Absorption Techniques

Direct observation of soil disturbance was also accomplished by means of X-ray absorption techniques being currently developed by Dr. A. H. Bouma of the Texas A&M University Oceanography Department. Radiograms were taken of samples obtained from regions of local shear failure, general shear failure, and undisturbed soil. The results of these analyses are shown in Figures 7.7 and 7.8. These prints show visually the extensive effects of local shear failure upon the soil structure in the case of the samples on the left and the general shear failure to which the center samples were subjected. Samples from undisturbed material are shown on the right for purposes of comparison.

The exact radial extent of the various disturbances cannot be established in this study by direct observation of soil samples due to the fact that the number of borings was limited in order to least affect excess pore water pressure measurements. However, direct observation by measurement of soil properties and X-ray absorption techniques indicates clearly the existence of the types of disturbances proposed in Chapter II within the regions where they are to be expected.

CHAPTER VIII

PORE WATER PRESSURE FLUCTUATIONS ASSOCIATED WITH SOIL FAILURE

Measurements Taken After Driving

The pore water pressure measurements, required to verify the proposed new theory presented in Chapter III of this study, were obtained by a continuous monitor of pore pressure transducers during driving and initial rise of pore pressures subsequent to driving. The dissipation process of the excess hydrostatic pore water pressure was recorded by means of a digital strain indicator over a period of approximately four weeks. A continuous record was also made of pore pressure changes during static load tests. Good data were obtained from three pressure transducers showing pore pressure fluctuations following driving and following static load tests to the ultimate bearing capacity of the pile. These pressure transducers were located at depths of thirty, forty, and fifty feet. Although a response can be noted in pore pressure transducer traces during driving, the trace displacements cannot be interpreted as true pressure readings, since they correlate with the magnitude of the stress wave rather than with any measurements of pore pressure indications to be logically expected. The dynamic response of the transducer is attributed to the sensitivity of the pressure diaphragm to transverse vibrations.

Pore pressure observations taken after driving are shown in Figures 8.1, 8.2, and 8.3, and in Tables B-1, B-2, and B-3, Appendix B. As shown in Figures 8.1 and 8.2, the pore pressure fluctuations in clay strata are as to be expected according to the envisioned soil disturbances presented in Figure 2.7. A rapid initial rise in pore pressures is noted upon completion of driving as pressures come to equilibrium within the region of local shear failure. It is considered that instrument readings during this time period may lag behind the true pressure fluctuations taking place away from the surface of the pile. This is logical since any variations in pore pressures must be accompanied by a finite volume change through the dense soil structure immediately adjacent to the pile surface in order to give an indicated transducer reading. A sharp drop in readings is indicated in clay at the 50 ft. level as shown in Figure 8.1 approximately

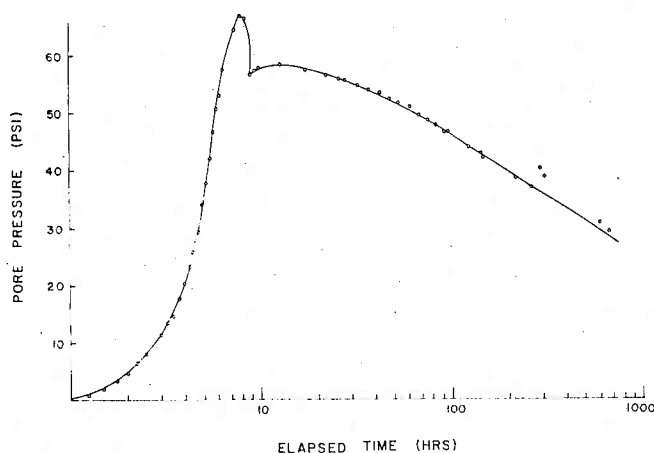


Figure 8.1: Pore pressure measurements in clay stratum—50' depth.

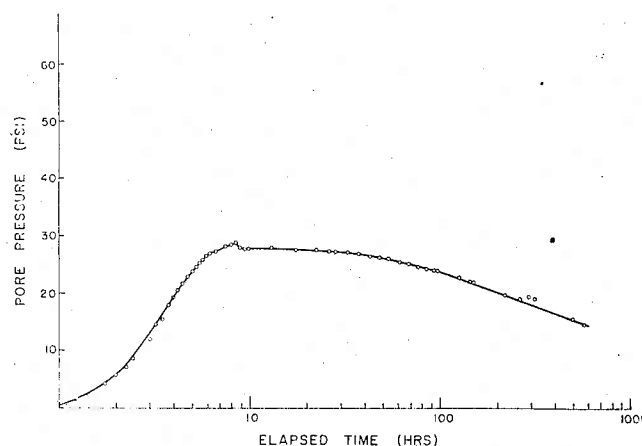


Figure 8.2. Pore pressure measurements in clay stratum 40' depth.

eight hours after completion of driving. The same pattern is repeated at a greatly reduced magnitude at the 40 ft. depth as presented in Figure 8.2. This apparently erratic drop in pore pressures may be attributed to some lateral relaxation of the soil because of borings taken during this time period. It is possible that an increase of all subsequent readings of pressure at the 50 ft. level by approximately 10 psi would present a better pattern of pressures to be expected had no borings been taken. Indicated pressures had peaked at the 50 ft. level prior to this erratic drop. It is felt that the maximum pressures observed in this study should be taken as indicative of the true maximum pressures reached, despite the effect of taking the soil borings.

The rise in pressure in Figures 8.1 and 8.2 at an elapsed time of approximately 310 hours are the effects of static load tests. A comparison of these peaks and subsequent dissipation patterns with the complete curve gives an insight into the relative magnitudes of soil disturbance associated with failures produced by dynamic

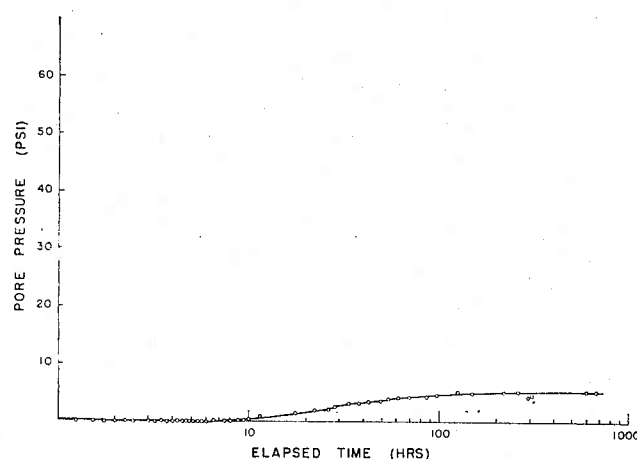


Figure 8.3. Pore pressure measurements in sand stratum 30' depth.

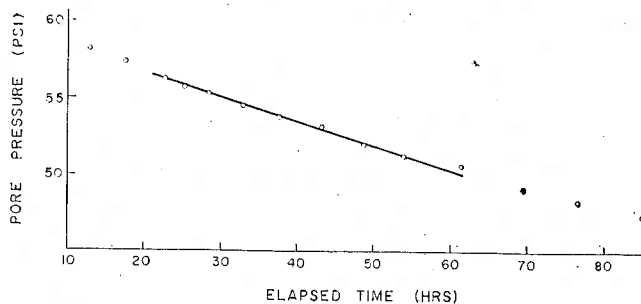


Figure 8.4. Initial pore pressure dissipation in clay stratum—50' depth.

and static loadings. Such comparisons lead to the assumed relative extents of soil disturbance presented in Figure 2.7 produced by failures due to static and dynamic loadings.

Figure 8.3 presents an interesting comparison of pressure fluctuations in sand stratum as opposed to clay. The over-all pattern of the curve in this case is a slow rise after driving with values approaching the hydrostatic head for this particular depth. A drop in values during the static load test is noted in this case.

Dissipation curves observed in clay strata are presented in the form of arithmetic plots in Figures 8.4 and 8.5 for the period of 10 to 80 hours. The plot of values observed at a depth of 50 ft. shown in Figure 8.4 has the steeper slope of the two as is to be expected according to Equation 3.14 with the greater pore pressures observed at this level. It may be noted that the values obtained at a depth of 40 ft. (Figure 8.5) produce a better straight line plot over a longer time interval than those obtained at 50 ft. In fact, the over-all pattern of the curve obtained at 50 ft. corresponds to values to be expected according to Soderberg's analysis. This is to be expected, since at this particular depth, a very small length of the pile has moved through the region of local shear failure. At the 40-ft. depth, on the other hand, a significant length of the pile has moved through this region and has produced a well developed flow pattern. Thus, the field observations of this study, in general, validate Soderberg's numerical analysis when conditions exist such that the physical model envisioned by Soderberg is reproduced. However, for the actual conditions along the length of the pile, observed pressures substantiate the proposed failure theory of soil disturbance as presented in Chapter II and of pore pressure fluctuations as presented in Chapter III.

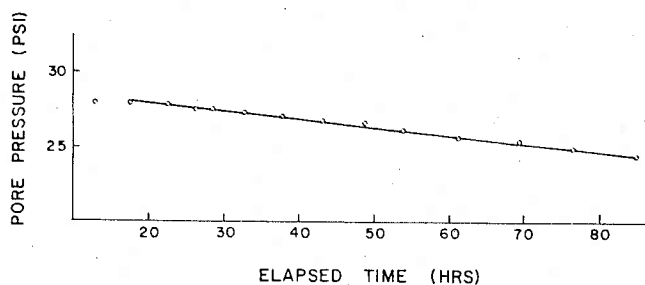


Figure 8.5. Initial pore pressure dissipation in clay stratum—40' depth.

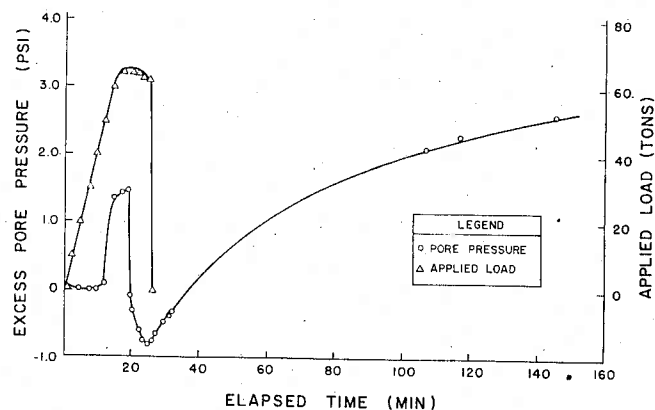


Figure 8.6. Excess pore water pressure due to static load test #1—50' depth.

Measurements Taken After Static Load Tests

Pore pressure fluctuations associated with the 13th day static load tests are presented in Figures 8.6 through 8.9, and Tables B-4, B-5, Appendix B. The 13th day test consisted of four loading cycles. Pore pressure measurements were made at the 50 foot depth during cycles No. 1 and 2, and at the 30-foot depth during cycles 3 and 4. It may be noted in the case of a clay stratum (50 ft. depth) as shown in Figures 8.6 and 8.7 that pore pressures rise with increased load until the pile plunges. Upon failure, the pore pressures drop until load is released. Then, as shown in Figure 8.6, after load release, pressures rise to a level higher than that which existed

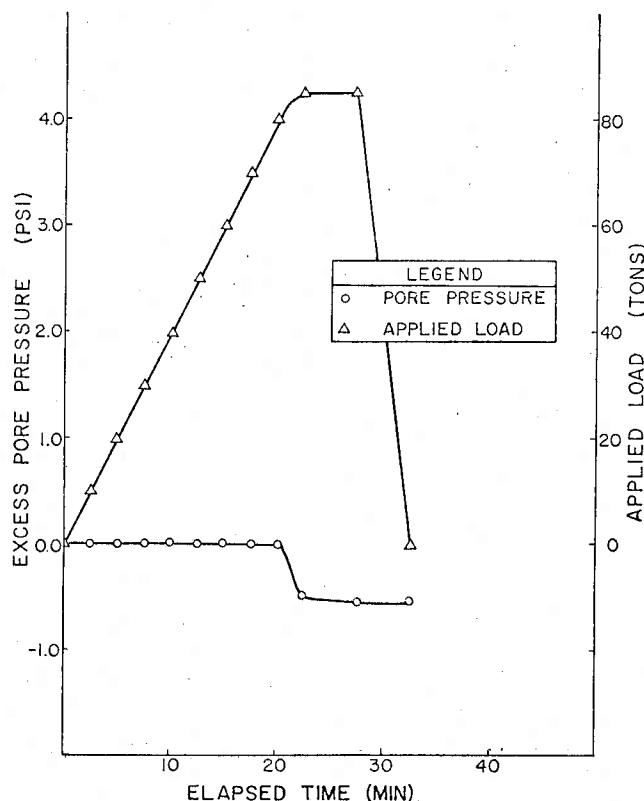


Figure 8.7. Excess pore water pressure due to static load test #2—50' depth.

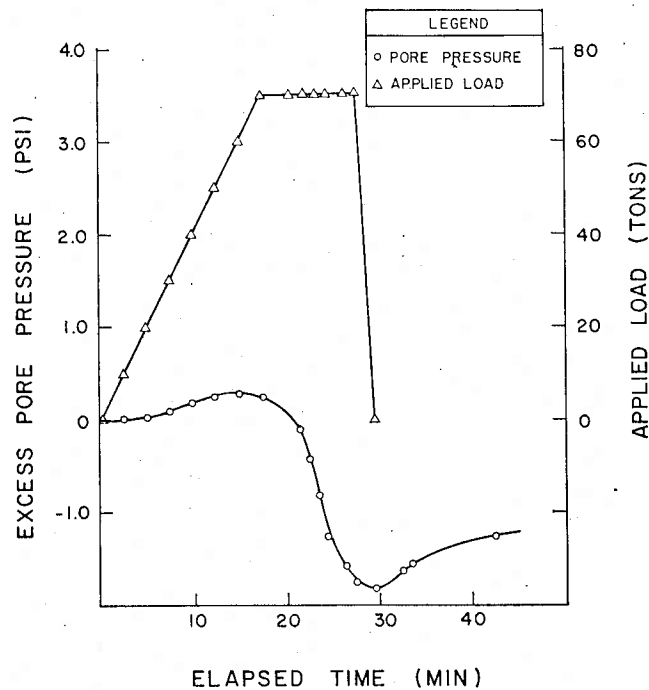


Figure 8.8. Excess pore water pressure due to static load test #3—30' depth.

prior to failure. A variation of pressures during load application as a function of prior disturbance through static failure may be noted from comparison of Figures 8.6 and 8.7. The excess pore pressures just prior to failure during the first load test are approximately 1.5 psi.

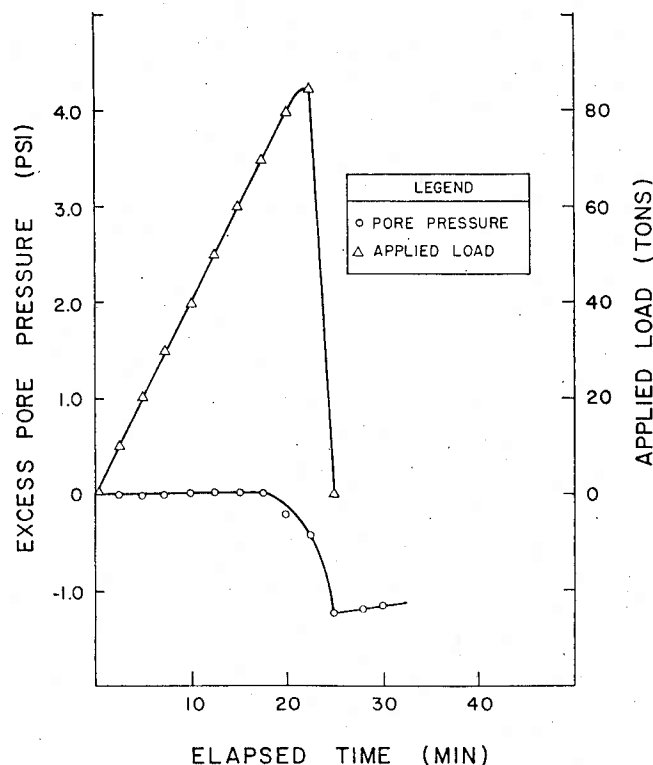


Figure 8.9. Excess pore water pressure due to static load test #4—30' depth.

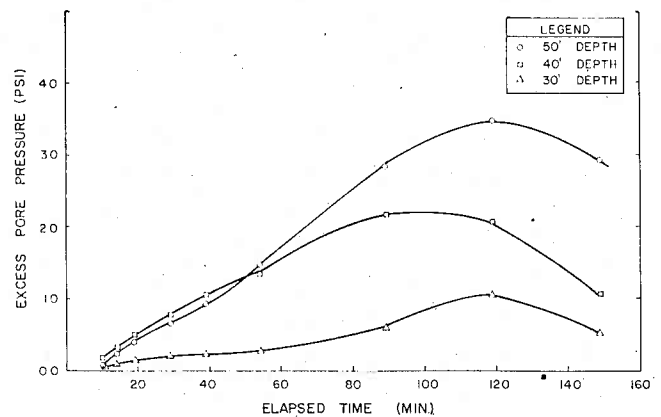


Figure 8.10. Peak pore pressures reached after static load tests.

Corresponding values attained during the second load test amount to only 0.3 psi. A sharp peak of pressures prior to yield in the first test compared to a slow rise during the second test may also be noted. These magnitudes and patterns of pore pressure rise prior to failure indicate that the first load test produced a fracture in the soil along the length of the pile. Subsequent load tests result in continuing movement in the disturbed soil along the same fracture pattern.

Pore pressure observations were made in sand strata (30-ft. depth) for static load tests during cycles 3 and 4 for purposes of comparison, and are presented in Figures 8.8 and 8.9. No rise is noted in pressures prior to fail-

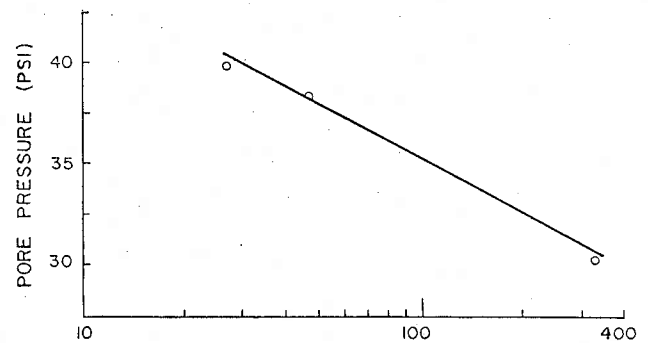


Figure 8.11. Pore pressure dissipation in clay stratum after load test—50' depth.

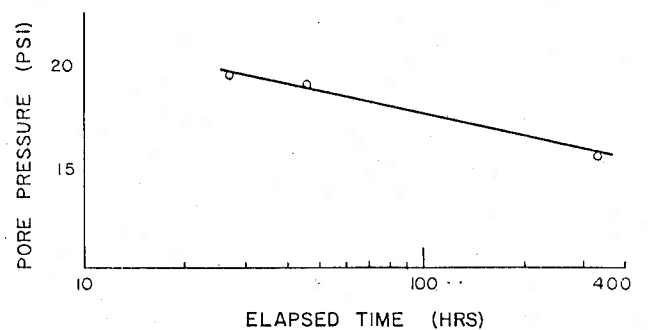


Figure 8.12. Pore pressure dissipation in clay stratum after load test—40' depth.

ure. when pore pressures exhibit a very sharp drop. This development of negative pore pressures may be attributed to volume expansion during shear failure in the sand.

Figure 8.10 and Table B-6, Appendix B presents a comparison of highest excess pressures reached after the 30th day static load test for various depths. The curves obtained at 50 ft. and 40 ft. were in clays while the 30 ft. depth was in a sand stratum.

Figures 8.11 and 8.12 and Table B-7, Appendix B, indicate the excess pore pressure dissipation patterns for the period between the 13th day test and the 30th day test. It can be noted that these curves approximate a straight line semi-logarithmic plot. This indicates that the excess pore pressures generated by static failures fall into the general dissipation patterns applicable to pressures resulting from the dynamic failures occurring during driving.

CHAPTER IX

RESPONSE OF THE PILE-SOIL SYSTEM TO STATIC AND DYNAMIC LOADING

Total Response During Driving

The ultimate load response developed by a pile-soil system as it yields in a failure mechanism is of both theoretical and practical importance. The concepts presented in Chapters II and IV of this study concerning the response of the pile-soil system were developed by measurements from an instrumented pile. These measurements included strain gage and accelerometer readings from the instrumented pile and a field total permanent set measurement for the pile with each hammer blow. These data were related to total soil response during driving by means of an existing computer program based upon the one dimensional wave equation.

As presented in Chapter II, the failure mechanism associated with a pile driven into a cohesive clay is considered to be composed of two components: Local Shear Failure and General Shear Failure as shown in Figure 2.7. The ultimate load response associated with the development of the general shear failure mechanism is transmitted to the pile in the form of point load. This component of the total response of the soil system could be measured directly by means of the strain gage bridge located just above the tip of the pile. Strain gage readings at a penetration of the 50 ft. indicated a maximum point load during driving of 72,000 lb.

In order to obtain a measure of the dynamic load response along the length of the pile, minor adaptations were made to the existing computer program in order to obtain computed values of accelerations at the tip. Then computed values of accelerations and stresses were compared to those measured in the field by accelerometer trace as corrected by observations of permanent set for each hammer blow.

The elastic deformation, or quake, of the soil along the length of the pile and at the pile point was taken as .01 in. for the computer solution. This value was determined by dynamic soil tests with friction pile models upon representative undisturbed samples taken at the site. The value of damping used in this particular analysis was arbitrarily set at 0.0 for both side friction and point bearing. Therefore, the computer printout obtained simulates values of the total dynamic response with no damping in the system. The distribution of the side friction of the soil system is based upon the unconfined shear strengths of soil strata corresponding to the 5 ft. segments used in the computer simulation of the mechanical elements of the pile-soil system. The distribution of the total soil resistance was proportioned to

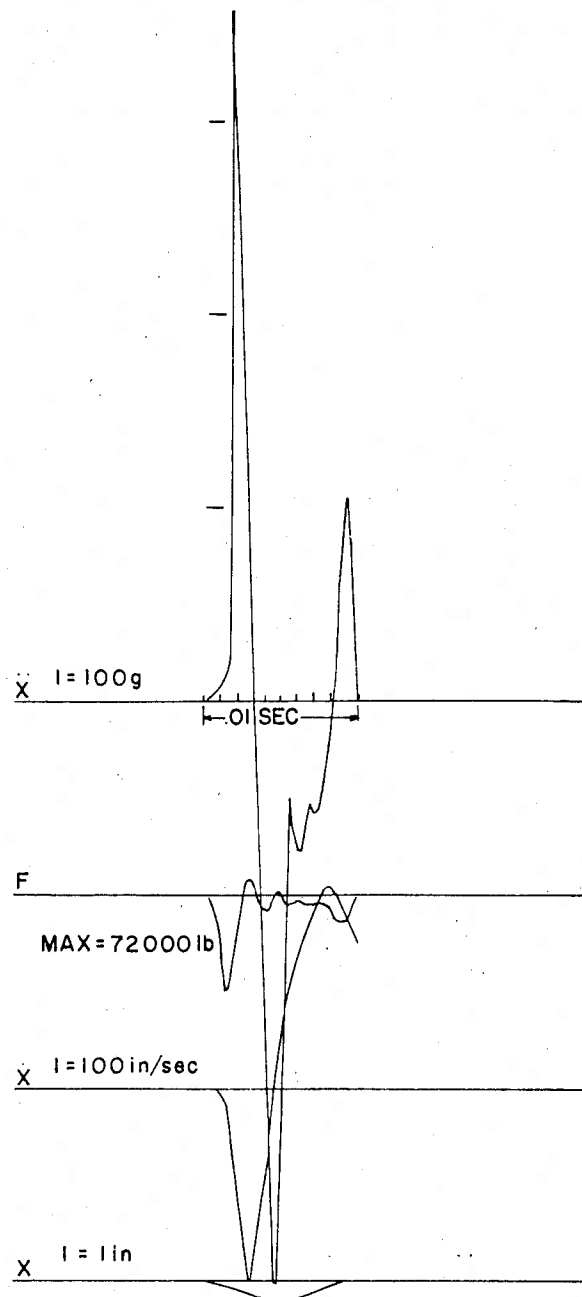


Figure 9.1. Field measurements of acceleration integrated to displacements.

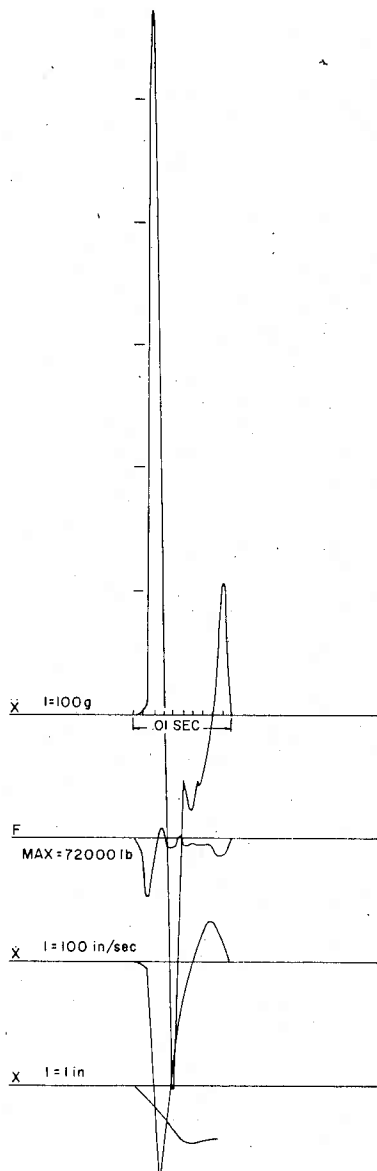


Figure 9.2. Corrected measurements of acceleration integrated to displacements.

obtain a point load response approximately equal to that measured by strain gages at the pile tip.

The acceleration readings chosen as appropriate for comparison with computed values were obtained from the 360 cycle/sec. accelerometer. It was determined that the response time of this type accelerometer was too slow to record the peak accelerations associated with the very high displacement wave velocities generated by the steel on steel contacts of the mechanical pile driving system. The fast response accelerometer recorded field values of acceleration of 360 g's. Computer calculations indicate that the total soil response during driving corresponding to these values of acceleration was 850,000 lbs. Stress magnitudes obtained by this computer simulation were much greater than measured values.

If these values of acceleration are integrated numerically to obtain values of velocity which can be similarly

used to obtain displacements, they would indicate a permanent set of 0.0 as shown in Figure 9.1. Since the values of set measured during the last blows of driving were on the order of .43 in., it is considered that the very rapid initial positive accelerations of the mechanical elements of the system were slightly faster than the instrument was capable of recording. The sharp peak of the trace tends to substantiate this conclusion. The rounded peak of the curve in the negative range of the first cycle indicates that the instrument recorded a value fairly close to the true peak. Readings following the second positive peak are considered to be vibrational response of the mechanical elements of the installation. If the initial positive peak is increased such that agreement is obtained with the observed permanent set due to each hammer blow, a value of approximately 575 g's is obtained for the initial positive acceleration as indicated in Figure 9.2. It is considered that this is close to the true acceleration existing in the field and the value which should be compared with computed values.

The total soil response during driving indicated by computer calculations which corresponds to a positive acceleration of approximately 575 g's and stresses recorded in the field is 650,000 lb. distributed according to Figure 9.3. The complete computer printout is presented in Appendix D. Since the computer printout indicates a permanent set of only .12 in., the value of damping existing in the field was some significant value rather than the value of zero used to obtain the simulated total dynamic response by computer calculation. This substantiates the hypothesis that the true total soil response during driving has a viscous friction component as well as a Coulomb friction component. A lower Coulomb friction component and some significant viscous friction component would give a greater set for the same total load response corresponding to the values of acceleration obtained. Such a rheological model has been proposed by Smith (30).

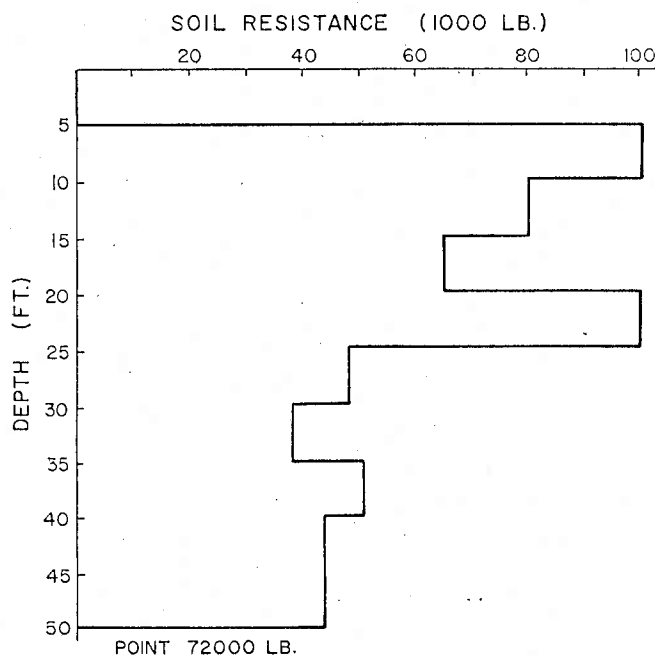


Figure 9.3. Maximum dynamic soil resistance upon each 5-ft. segment.

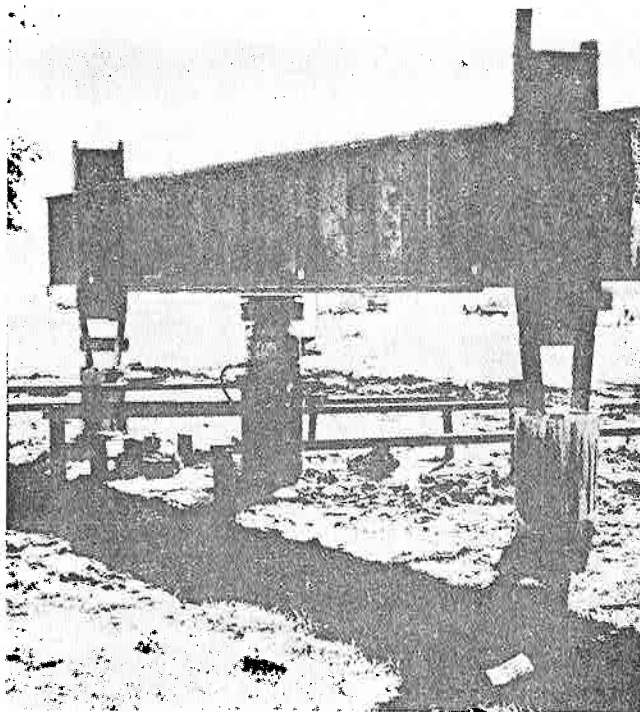


Figure 9.4. Static load test equipment.

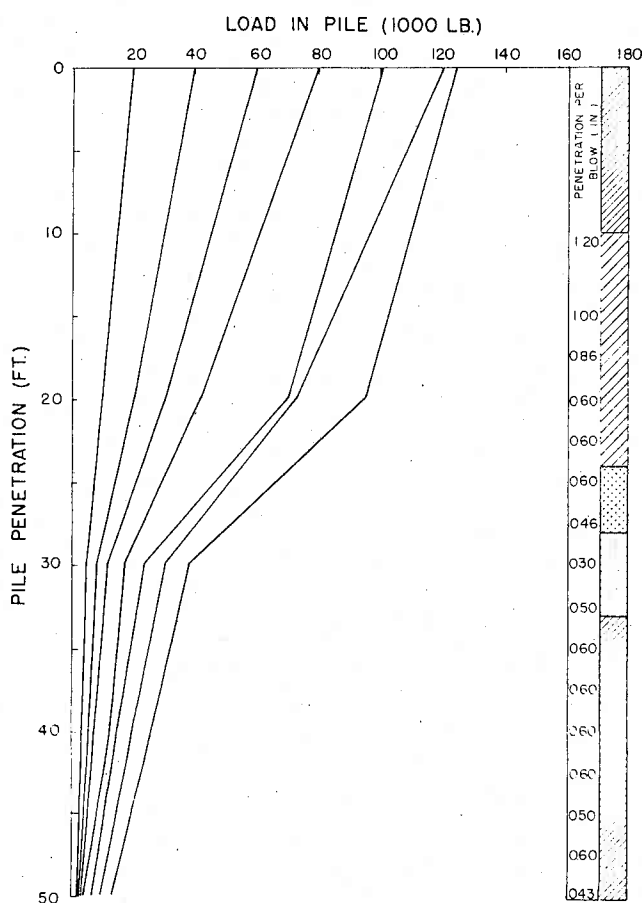


Figure 9.5. Load transfer curves 13 days after driving —test #1.

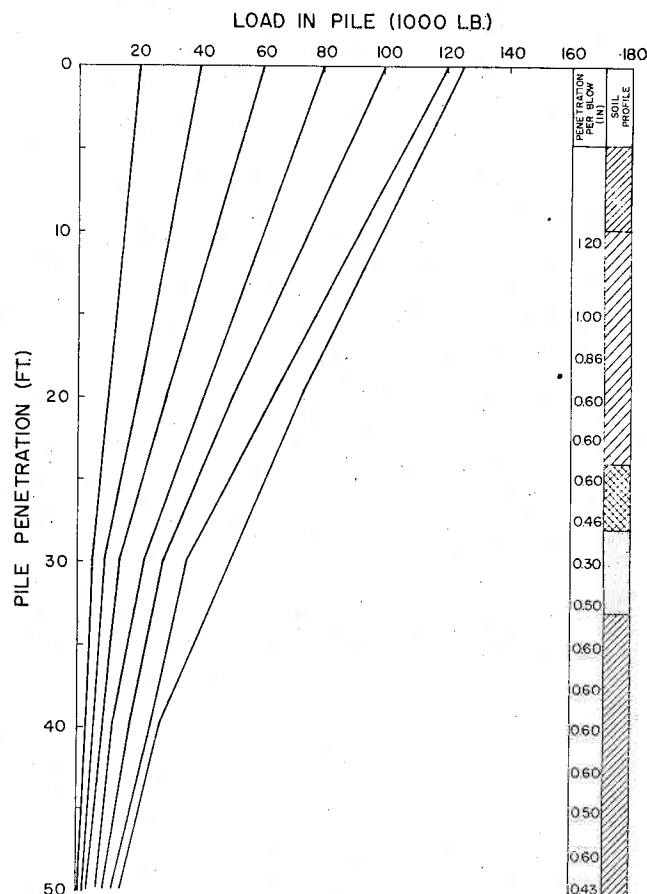


Figure 9.6. Load transfer curves 13 days after driving —test #2.

Static Load Response Changes with Time

Static load tests were conducted to determine ultimate bearing capacity of the test pile. Procedures and load test equipment (see Figure 9.4) were in keeping with standard Texas Highway Department practice. Ultimate bearing capacity, as determined by static load tests, was used in this study to evaluate changes in soil response with time and to obtain a measure of the load carrying capacity of the various strata along the length of the pile. Information from these tests can be used in relating the various laboratory measurements of soil properties to the static field response of the system. By using load test results in this manner, the effects of core sampling upon the study of the load response of the system is considered to be minimized. Since soil conditions in the area are relatively uniform, two other load tests performed on the project were also used in investigating these effects.

Load transfer data developed by load tests are shown in Figures 9.5 to 9.8 and Tables C-1, C-2, C-3, and C-4. Appendix C. Values recorded electronically have been adjusted to match load indications of the calibrated hydraulic loading jack. The ultimate bearing capacity which could be expected according to soil tests indicates that a significant lowering in bearing capacities resulted from taking a boring adjacent to the test pile (see Figure 2.7, boring A and C). A similar conclusion is indicated by comparison with results obtained from other load

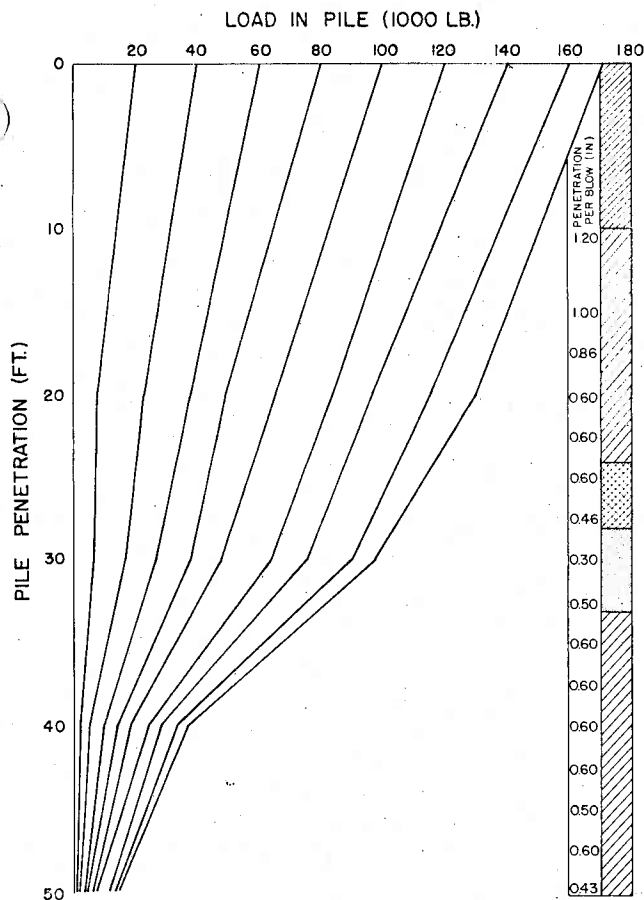


Figure 9.7. Load transfer curves 30 days after driving test #1.

tests conducted on the same project. Other test piles driven to depths of 46 and 47.5 ft. penetration developed ultimate loads of 220,000 lb. and 260,000 lb., respectively. Simple skin friction computed from values obtained in unconfined shear strength determinations indicated an ultimate bearing capacity of approximately 300,000 lb. Despite the decrease in over-all load bearing capacity, the load transfer curves demonstrate the increase of static load carrying capacity with time. An ultimate bearing capacity of 170,000 lb. was recorded 30 days after driving as compared to only 124,000 lb. recorded 13 days after driving. This increase occurs with time as consolidation and thixotropic hardening of the disrupted soil structure takes place.

A maximum point load of approximately 20,000 lb. was developed during static failure as compared with

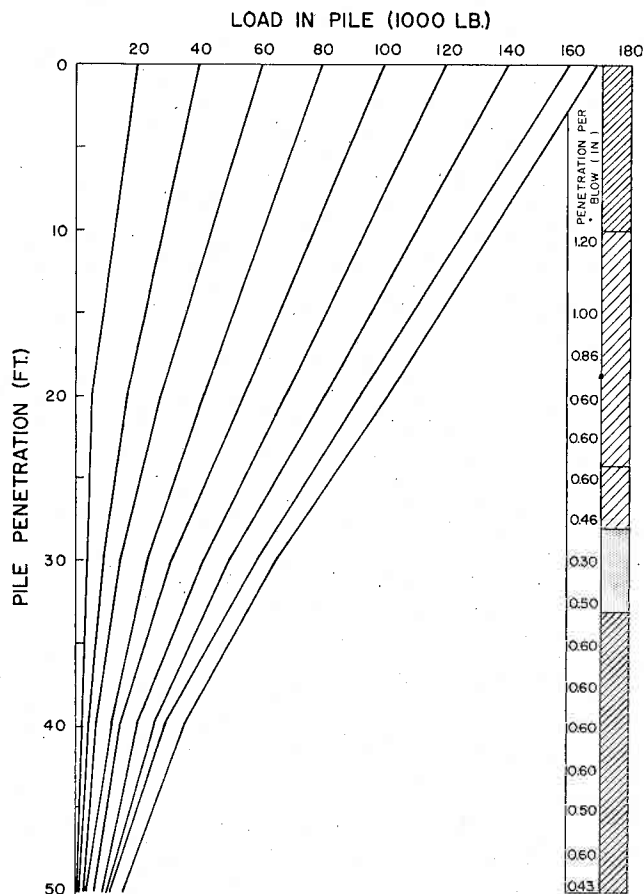


Figure 9.8. Load transfer curves 30 days after driving test #2.

72,000 lb. during driving. Since the load response of the general shear failure mechanism is transmitted to the pile as point load, this comparison indicates the greater dimensional extent of soil involved in the mechanism developed by dynamic loading as opposed to static loading. The dynamic point load includes some inertial effects of the soil mass which would result in a higher point load than developed by a static yield of the same dimensional extent of soil. This relative increase in the dynamic point load may be lowered somewhat due to the fact that the soil is in a disturbed condition during driving compared to its condition at the time static load tests were performed. However, these comparative values substantiate qualitatively the theory as presented in Chapter II. Application of load to the same material at a slower rate of loading results in a less extensive general shear failure mechanism.

CHAPTER X

CONCLUSIONS

Reiterating the conclusions of the different types of observations:

1. The soil disturbances measured in this study correspond to those which could be expected to develop according to the failure mechanisms presented in Chapter II. This conclusion is based on direct observations,

determination of soil properties of samples taken from borings, and from plots of initial excess pore water pressure dissipation. The behavior of cohesive soil subjected to loads associated with pile driving in this study approached the ideal elastic-plastic model as indicated by Figures 3.1 and 7.1.

2. Observed pore pressure measurements at the pile surface verify the concepts presented in the proposed new theory of Chapter III. After the initial pore pressure rise, as pressures equalize within the region of local shear failure, dissipation takes the form of a straight line plot as water movement occurs predominantly from the region of local shear failure to that of general shear failure. Thereafter, dissipation patterns approach a semilogarithmic plot resembling a consolidation curve.

3. Load response is presented in Chapter IV. Both static and dynamic load responses for the pile-soil system considered in this study are a function predominantly of the soil properties within the region of local shear failure.

CHAPTER XI

RECOMMENDATIONS

Practical Applications of Study Results

In the opinion of the authors, the most important single result of this study has been the development of a mode of failure for a cohesive soil involved in the load response of a pile-soil system. This failure mechanism has been described by an analytic approach and substantiated by the correlation of results obtained by various field measurements. The formulation of such a failure mechanism should contribute to future research by giving direction to investigations into various single aspects of the total response of the pile-soil system. Some conclusions of this study, however, offer immediate practical application. Consideration should be given to the fact that the dimensional extent of soil disturbance which governs the magnitude and duration of excess pore pressures is a function of the square of the radius. This leads to the conclusion that revisions of some aspects of current load test procedures might well be considered. Specifications currently require that load tests performed in order to establish ultimate bearing capacities for piling design be accomplished after a given number of days. These should possibly be altered to recognize the fact that large diameter piles require a much longer period in order to attain their ultimate bearing capacity than small piles driven into similar soil. On the basis of Equation 3.14, for similar soil conditions, the time required for piles of different radii to attain comparable percentages of their ultimate bearing capacity is expressed by the dimensionless ratio:

$$\frac{r_1^2}{r_2^2} = \frac{T_1}{T_2} \quad (11.1)$$

where: r_1 = radius of pile 1

r_2 = radius of pile 2

T_1 = time for pile 1 to attain a stated percentage of ultimate load capacity

T_2 = time for pile 2 to attain same percentage

Verification of the elastic-plastic model as the most appropriate description of the behavior of the soil considered in this study indicates that the soil disturbances associated with local shear failure are limited to a distance from the center of the pile expressed by the dimensionless ratio:

$$\frac{r}{r_1} < 4.5 \quad (11.2)$$

where: r = radial distance from pile center
 r_1 = radius of pile

The dissipation of excess pore water pressures from around large piles has been determined by this study to be a more complex process than that presented by previous mathematical models. The fact that an exponential increase in bearing capacity of large piles does not start immediately upon cessation of driving should be considered in construction loading. It should be recognized that the disparity between these findings and those previously obtained for small piles is due to the fact that the dimensional effects of local shear failure are masked in small diameter piles since a negligible volume of soil is subjected to local shear failure.

Suggestions for Future Research

This study has indicated several areas requiring future research. It is first suggested that comparable field tests be performed in similar soils in order to establish the reliability and generality of the results obtained in this study. It is suggested that such investigations be performed upon specific areas covered in this study rather than duplicate the entire spectrum of response with which this research was concerned. Such procedures will eliminate the interference, for example, of soil borings with measurements of ultimate bearing capacities.

One area requiring research is in the field of model studies and the correlation of static and dynamic model tests with the field response of full scale piles. Refinement of such techniques would greatly enhance the overall research effort in this area by enabling investigators to obtain more information from each costly field test. The future requirement of full scale field tests, however, to substantiate laboratory work is not to be minimized.

It should be recognized in dealing with this problem that a static response as determined by any analysis of dynamic response is developed according to a dynamic mode of failure. This failure mechanism is essentially different from the mode of failure developed during the slower static failure. It is suggested that more research be accomplished in order to correlate these two failure mechanisms by means of pore pressure measurements.

References

1. Barkan, D. D., *Dynamics of Bases and Foundations*, McGraw-Hill Book Company, New York, translated 1960.
2. Baver, L. D., *Soil Physics*, John Wiley and Sons, New York, 1956.
3. Brothie, John F., "Elastic-Plastic Analysis of Transversely Loaded Plates," *Journal of Engineering Mechanics Division*, Proceedings of the American Society of Civil Engineers, October, 1960.
4. Carslaw and Jaeger, J. D., *Conduction of Heat in Solids*, Oxford University Press, Oxford, 1947.
5. Casagrande, Arthur, "The Structure of Clay and Its Importance in Foundation Engineering," *Contributions to Soil Mechanics*, Boston Society of Civil Engineers, Boston, 1948, pp. 72-125.
6. Chan, Paul C., "A Study of Dynamic Load-Deformation and Damping Properties of Sands Concerned with a Pile-Soil System," Dissertation, Texas A&M University, 1967.
7. Chellis, Robert, *Pile Foundations*, McGraw-Hill Book Company, New York, 1951.
8. Cummings, A. E., "Dynamic Pile Driving Formulas," *Journal of the Boston Society of Civil Engineers*, Boston, 1940.
9. Cummings, A. E., Kerkhoff, G. O. and Peck, K. B., "Effect of Driving Piles into Soft Clay," *Transactions American Society of Civil Engineers*, Vol. 115, 1950, pp. 275-350.
10. Den Hartog, J. P., *Advanced Strength of Materials*, McGraw-Hill Book Company, New York, 1952.
11. Forehand, Paul W. and Reese, Joseph L., *Pile Driving Analysis Using the Wave Equation*, Master's Thesis, Princeton University, 1963.
12. Frederick, Daniel, "On Some Problems in Bending of Thick Circular Plates on an Elastic Foundation," *Journal of Applied Mechanics*, June, 1956.
13. Glanville, W. H., et al., "An Investigation of the Stresses in Reinforced Concrete Piles During Driving," *British Building Research Board Technical Paper No. 20*, Dept. of Scientific and Industrial Research, His Majesty's Stationery Office, London, 1932.
14. Grim, Ralph, *Clay Mineralogy*, McGraw-Hill Book Company, New York, 1953.
15. Hirsch, Teddy J., "A report on Field Tests of Prestressed Concrete Piles During Driving," Texas Transportation Institute, Texas A&M University, unpublished.
16. Hirsch, T. J. and Edwards, T. C., "Use of the Wave Equation to Predict Pile Load Bearing Capacity," Texas Transportation Institute, Texas A&M University, unpublished.
17. Icaas, D. V., "Reinforced Concrete Pile Formulae," *Transactions, Institute of Engineers*, Australia, Vol. 12, 1931.
18. Jungenson, Leo, "The Application of Theories of Elasticity and Plasticity to Foundation Problems," *Contributions to Soil Mechanics*, Boston Society of Civil Engineers, Boston, 1940, pp. 148-183.
19. Kondner, R. L., "A Rheologic Investigation of the Dynamic Response Spectra of Cohesive Soils," Contract Report, U. S. Army Engineer Waterways Experiment Station, Vicksburg, Mississippi, 1966.
20. Meyerhof, G. G., "The Ultimate Bearing Capacity of Foundations," *Geotechnique*, Vol. II, Number 4, Dec., 1951, pp. 301-332.
21. Mohr, O., *Abhandlungen aus den Gebiete der Technischen Mechanik*, 3rd ed., W. Ernst and Sohn, 1928.
22. Nadai, A., *Theory of Flow and Fracture of Solids*, 2nd Edition, McGraw-Hill Book Company, 1950.
23. Pauw, "Symposium on Dynamic Testing of Soils," *ASTM Spec Tech. Publ. 156*, 1953.
24. Raba, Carl F., Unpublished Dissertation, Texas A&M University, January, 1968.
25. Reese, L. C. and Seed, H. B., "Pressure Distribution Along Friction Piles," *Proceedings, American Society for Testing Materials*, Vol. 55, 1955.
26. Reissner, E., "Stationare, axidsymmetrische durch ein scutheimde mass e-egte Schwingungen eines homogeneu elastischen Halbeaumes," *Ingenieur-Archiv*, Vol. 7, 1936, pp. 381-396.
27. Samson, Charles H., Jr., Hirsch, Teddy J. and Lowery, Lee L., Jr., "Computer Study of Dynamic Behavior of Piling," Third Conference of Electronic Computation, ASCE, Boulder, Colorado, June, 1963.
28. Samson, Charles H., Jr., "Pile-Driving Analysis by the Wave Equation (Computer Application)," Report of the Texas Transportation Institute, A&M College of Texas, 1962.
29. Smith, E. A. L., "Impact and Longitudinal Wave Transmission," *Transactions, ASME*, August, 1955, p. 963.
30. Smith, E. A. L., "Pile-Driving Analysis by the Wave Equation," *Journal of the Soil Mechanics and Foundations Division*, Proceedings of the American Society of Civil Engineers, Vol. 86, No. SM 4, 1960, pp. 35-61.
31. Soderberg, Lars, "Consolidation Theory Applied to Foundation Pile Time Effects," *Geotechnique*, Vol. XII, Number 3, Sept., 1962, pp. 217-225.
32. Terzaghi, Karl and Peck, Ralph, *Soil Mechanics in Engineering Practice*, John Wiley and Sons Inc., New York, 1948.
33. Terzaghi, Karl, Presidential Address, *Proceedings First International Conference on Soil Mechanics and Foundation Engineering*, Cambridge, Massachusetts, 1936.
34. Terzaghi, Karl, *Theoretical Soil Mechanics*, John Wiley and Sons Inc., New York, 1943.

35. Terzaghi, Karl. "The Shearing Resistance of Saturated Soils," *Proceedings First International Conference on Soil Mechanics*, Vol. I, Cambridge, Mass., 1936, pp. 54-56.
36. Thompson, L. J., *Dynamic Penetration of Selected Projectiles into Particular Media*, Sandia Laboratory, Albuquerque, 1966.
37. Timoshenko, S. P. and Goodier, J. N., *Theory of Elasticity*, 2nd Edition, McGraw-Hill Book Company, New York, 1951.
38. Timoshenko, S. P. and Woinowsky-Krieger, S., *Theory of Plates and Shells*, 2nd Edition, McGraw-Hill Book Company, New York, 1959.
39. Timoshenko, S. P., *Vibration Problems in Engineering*, D. Van Nostrand Company, New York, 3rd Edition, 1955.

Appendix A

SOIL PROPERTY DATA

Table A - 1
VANE SHEAR — FIG. 7.2

Depth (ft)	Boring - D Undisturbed (psf)	Boring - A Local Shear Lab (psf)	Boring - B General Shear Lab (psf)	Boring - C Local Shear Consolidated (psf)	Boring - A Local Shear Field (psf)	Boring - B General Shear Field (psf)
5-7.5	1750 2750			1100		1910
7.5-10	1930	2180		1700	2350	
10-12.5	1700	2000		1550	2800	1810
12.5-15	900			1700	1070	
15-17.5	740	3100		1800	1700	
17.5-20		1300	1750		800	3080
20-22.5			3000	2600		
22.5-25			1340		2500	
25-32.5	Sand	Sand	Sand	Sand	Sand	Sand
32.5-35		1650		1590		
35-37.5	1650	1200	1120	1820	1620	
37.5-40	1690	1000		1300	1200	1720
					2000	
40-42.5					1130	1300
42.5-45	1350	1200	1400	1620	1100	
45-47.5	1540	1150	1350	1410	1120	1400
47.5-50	1550	1200	1600	1700	940	1500
					1200	
50-52.5		1610			1100	

Table A - 2
UNCONFINED SHEAR STRENGTH — FIG. 7.3

Depth (ft)	Boring - A Local Shear (psf)	Boring - C Local Shear Consolidated (psf)	Boring - B General Shear (psf)	Boring - D Undisturbed (psf)
10	3200			
10-12.5	2600	1900		1700
12.5-15	1100			
15-17.5	2700			
17.5-20	1600		1370	
20-22.5	2550	2350	2050	2750
22.5-25	4000			
25-27.5			1150	1500
27.5-32.5	Sand	Sand	Sand	Sand
32.5-35	1500	950		2270
35-37.5	1600	1500	1650	1850
37.5-40	1550	1020		2230
40-42.5				
42.5-45	1300	1980	1875	1900
45-47.5	1300	1980	2150	1980
47.5-50	1400	2600		2900
50-52.5	1850		2650	

Table A - 3
DRY UNIT WEIGHT — FIG. 7.4

Depth (ft)	Boring - A Local Shear (pcf)	Boring - C Local Shear Consoli- dated (pcf)	Boring - B General Shear (pcf)	Boring - D Undis- turbed (pcf)
5.5	107.5			99.5
6.5		98.0		
9	100.0	100.0		91.0
10	100.0			
11				91.0
12	97.0	99.0		
14		85.0		96.0
17	94.0	96.0		98.0
18		96.0		
19	96.0		105.0	
21	100.0	107.0		
22			107.0	
23				107.0
25	110.0		100.0	
26				101.0
31				104.0
35	83.0	75.0		71.0
37	74.0	67.0	71.0	73.0
39	70.0	62.0		68.0
42		61.0		
43			61.0	
44	60.0			60.0
47		66.0	63.0	62.0
48	61.5	81.0		64.5
50			100.0	
52	92.0			

Table A - 4
MOISTURE CONTENT — FIG. 7.5

Depth (ft)	Boring - A Local Shear (%)	Boring - C Local Shear Consoli- dated (%)	Boring - B General Shear (%)	Boring - D Undis- turbed (%)
5-6	22.0			25.0
7-8		27.5		
8-10	26.0	27.0		26.5
10-12	28.0	26.5		26.0
13-15		28.0		27.0
17-19	25.0	26.5	25.0	24.0
	28.0	26.5		32.5
20-22	22.5	21.0	20.0	22.0
22-25	18.0		25.0	23.0
25-32	Sand	Sand	Sand	Sand
34-35	38.0	43.0		45.0
36-38	47.0	55.0	51.0	51.0
	51.0	60.0		57.0
42-45	67.0	64.5	67.5	67.5
47-50	59.5	57.0	62.0	63.5
	62.0	38.0	25.0	54.0
50-52	40.0			

Appendix B

PORE PRESSURE DATA

Table B - 1
PORE PRESSURE DATA — 50-FOOT DEPTH
(Fig. 8.1)

Elapsed Time (hrs.)	Pore Pres- sure (psi)	Elapsed Time (hrs.)	Pore Pres- sure (psi)	Elapsed Time (hrs.)	Pore Pres- sure (psi)
1:15	1.0	6:15	53.0	70:00	49.2
1:30	2.0	6:35	57.3	77:00	48.2
1:45	3.4	7:30	64.3	85:00	47.4
2:00	4.8	8:00	66.8	94:00	46.2
2:15	6.3	8:30	66.2	97:00	46.2
2:30	8.0	9:00	56.6	126:00	43.7
3:00	11.2	9:30	57.3	144:00	42.5
3:15	13.2	10:00	57.8	145:00	41.9
3:30	14.8	13:00	58.2	220:00	38.2
3:45	17.8	17:45	57.2	260:00	36.7
4:00	20.2	22:45	56.2	295:00	39.8
4:15	23.3	26:15	55.8	310:00	38.5
4:30	25.8	28:30	55.3	600:00	30.1
4:45	29.4	33:00	54.5	670:00	28.8
5:00	34.0	38:00	53.8		
5:15	37.8	43:00	53.2		
5:30	42.0	49:00	52.0		
5:45	46.5	54:00	51.4		
6:00	50.8	62:00	50.8		

Table B - 2
PORE PRESSURE DATA — 40-FOOT DEPTH

Elapsed Time (hrs.)	Pore Pres- sure (psi)	Elapsed Time (hrs.)	Pore Pres- sure (psi)	Elapsed Time (hrs.)	Pore Pres- sure (psi)
1:15	1.5	6:00	26.7	43:00	26.8
1:30	2.2	6:15	27.0	49:00	26.2
1:45	4.0	6:35	27.6	54:00	26.0
2:00	5.8	7:30	28.2	62:00	25.8
2:15	7.0	8:00	28.7	69:00	25.2
2:30	8.8	8:30	29.0	77:00	24.9
3:00	12.0	9:00	28.0	85:00	24.4
3:30	14.8	9:20	27.9	94:00	24.1
3:45	15.5	9:35	27.9	97:00	24.0
4:00	19.1	10:00	27.9	128:00	22.8
4:15	20.7	13:00	28.0	145:00	22.1
4:30	21.8	17:45	27.8	150:00	22.0
4:45	23.0	22:45	27.7	220:00	19.9
5:00	24.0	26:15	27.5	262:00	19.0
5:15	24.8	28:15	27.5	295:00	19.4
5:30	25.4	33:00	27.1	310:00	19.0
5:45	26.0	38:00	27.0	600:00	15.7
				670:00	14.9

Table B - 3
PORE PRESSURE DATA — 30-FOOT DEPTH
(Fig. 8.3)

Elapsed Time (hrs.)	Pore Pressure (psi)	Elapsed Time (hrs.)	Pore Pressure (psi)	Elapsed Time (hrs.)	Pore Pressure (psi)
1:15	0.0	5:45	0.0	43:00	3.6
1:30	0.0	6:00	0.0	49:00	3.8
1:45	0.0	6:15	0.0	54:00	4.0
2:00	0.0	6:35	0.1	62:00	4.1
2:15	0.0	7:30	0.1	70:00	4.2
2:30	0.0	8:00	0.1	86:00	4.5
3:00	0.0	8:30	0.1	94:00	4.7
3:15	0.0	9:00	0.1	98:00	4.8
3:30	0.0	9:15	0.1	127:00	5.1
3:45	0.0	9:30	0.1	145:00	4.9
4:00	0.0	10:00	0.3	150:00	5.0
4:15	0.0	17:45	1.8	220:00	5.0
4:30	0.0	22:45	2.0	260:00	5.1
4:45	0.0	26:15	2.0	295:00	4.4
5:00	0.0	28:45	2.7	310:00	4.8
5:15	0.0	33:00	3.2	600:00	5.1
5:30	0.0	38:00	3.3	670:00	5.1

Table B - 7
PORE PRESSURE DATA—TIME PERIOD (13th DAY
TO 30th DAY)
(Fig. 8.11 and Fig. 8.12)

Elapsed Time (hrs.)	40-Ft. Depth Pore Pressure (psi)	50-Ft. Depth Pore Pressure (psi)
27:00	19.5	39.8
46:00	19.0	38.4
330:00	15.5	30.2

Table B - 5
PORE PRESSURE DATA—STATIC TEST (13th DAY)
30-Foot Depth

TEST NO. 3 (Fig. 8.8)			TEST NO. 4 (Fig. 8.9)		
Elapsed Time (min)	Applied Load (tons)	Pore Pressure (psi)	Elapsed Time (min)	Applied Load (tons)	Pore Pressure (psi)
0	0	0	0	0	0
2:30	10	0	2:30	10	0
5:00	20	0	5:00	20	0
7:30	30	0	7:30	30	0
10:00	40	0	10:00	40	0
12:30	50	0	12:30	50	0
15:00	60	0	15:00	60	0
17:30	70	0	17:30	70	0
20:00	80	0	20:00	80	-0.20
22:30	85	-0.48	22:30	85	-0.40
27:30	85	-0.55	25:00	0	-1.22
32:30	0	-0.52	28:00		-1.20
			30:00		-1.15

Table B - 4
PORE PRESSURE DATA—STATIC TEST (13th DAY)
50-Foot Depth

TEST NO. 1 (Fig. 8.6)			TEST NO. 2 (Fig. 8.7)		
Elapsed Time (min)	Applied Load (tons)	Pore Pressure (psi)	Elapsed Time (min)	Applied Load (tons)	Pore Pressure (psi)
0	0	0	0	0	0
2:15	10	0	2:30	10	0
5:00	20	0	5:00	20	0.05
8:00	30	0	7:30	30	0.10
10:00	40	0	10:00	40	0.20
12:00	50	0.10	12:30	50	0.25
15:00	60	1.35	15:00	60	0.30
18:00	65	1.40	17:30	70	0.25
19:00	65	1.45	21:30	70	-0.10
19:45	64	-0.10	22:30	70	-0.45
20:00	64	-0.30	23:30	70	-0.82
22:00	63	-0.60	24:30	70	-1.25
24:00	62	-0.75	26:30	70	-1.60
25:00	0	-0.80	27:30	70	-1.75
26:00		-0.73	29:30	0	-1.85
28:00		-0.62	32:30		-1.63
30:00		-0.50	33:30		-1.55
31:30		-0.38	42:30		-1.25
32:00		-0.30			
108:00		2.10			
118:00		2.30			
148:00		2.60			

Table B - 6
PORE PRESSURE DATA—AFTER 30th DAY STATIC
TEST (Fig. 8.10)

Elapsed Time (min)	30-Ft. Depth Pore Pressure (psi)	40-Ft. Depth Pore Pressure (psi)	50-Ft. Depth Pore Pressure (psi)
10:00	0.02	0.18	0.08
14:00	0.10	0.22	0.32
19:00	0.11	0.50	0.40
29:00	0.20	0.78	0.65
39:00	0.22	1.05	0.92
34:00	0.28	1.32	1.48
89:00	0.60	2.18	2.83
119:00	1.05	2.06	3.48
149:00	0.52	1.08	2.92

Appendix C

LOAD TRANSFER DATA

Table C - 1
LOAD TRANSFER DATA—FIG. 9.5
13th DAY STATIC LOAD TEST NO. 1

Depth Below Ground Surface (ft.)	Load (kips)	Load (kips)	Load (kips)	Load (kips)	Load (kips)	Load (kips)	Load (kips)
0	20.0	40.0	60.0	80.0	100.0	120.0	125.0
10	15.0	30.0	45.0	61.0	85.0	97.0	110.0
20	10.0	25.0	30.0	42.0	71.0	73.0	95.0
30	5.0	8.0	11.0	17.0	24.0	30.0	38.0
40	3.0	5.5	7.0	12.5	15.0	20.0	25.5
50	2.0	2.0	3.0	4.5	7.0	10.0	18.0

Table C - 2
LOAD TRANSFER DATA—FIG. 9.6
13th DAY STATIC LOAD TEST NO. 2

Depth Below Ground Surface (ft.)	Load (kips)	Load (kips)	Load (kips)	Load (kips)	Load (kips)	Load (kips)	Load (kips)
0	20.0	40.0	60.0	80.0	100.0	120.0	125.0
10	15.0	30.0	45.0	60.0	75.0	87.0	100.0
20	10.0	20.0	29.5	41.0	50.5	63.5	72.5
30	5.0	9.5	14.5	21.0	28.0	35.5	50.0
40	2.5	5.0	4.5	12.0	17.0	24.0	26.0
50	0.5	2.0	3.5	6.0	9.5	12.0	15.0

Table C - 3
LOAD TRANSFER DATA—FIG. 9.7
30th DAY STATIC LOAD TEST NO. 1

Depth Below Ground Surface (ft.)	Load (kips)	Load (kips)	Load (kips)	Load (kips)	Load (kips)	Load (kips)	Load (kips)	Load (kips)	Load (kips)
0	20.0	40.0	60.0	80.0	100.0	120.0	140.0	160.0	171.0
10	14.0	32.0	50.0	65.0	83.5	104.0	120.0	138.0	151.0
20	7.5	23.0	38.0	50.0	65.0	85.0	97.0	117.0	130.0
30	6.0	16.0	27.0	38.0	48.0	64.0	75.0	91.0	99.0
40	2.0	5.0	10.0	15.0	19.0	25.0	30.0	35.0	39.0
50	1.0	2.0	3.5	4.5	5.5	6.5	10.5	13.0	15.0

Table C - 4
LOAD TRANSFER DATA—FIG. 9.8
30th DAY STATIC LOAD TEST NO. 2

Depth Below Ground Surface (ft.)	Load (kips)	Load (kips)	Load (kips)	Load (kips)	Load (kips)	Load (kips)	Load (kips)	Load (kips)	Load (kips)
0	20.0	40.0	60.0	80.0	100.0	120.0	140.0	160.0	169.0
10	12.5	28.0	44.0	60.0	77.0	95.0	110.5	120.0	135.0
20	5.0	16.0	27.0	40.5	55.0	68.0	80.0	91.0	100.0
30	3.0	9.0	15.0	23.0	31.0	41.0	50.0	59.0	65.0
40	2.0	4.0	6.0	11.0	15.0	20.0	25.0	29.0	35.0
50	0.5	1.0	2.5	3.0	5.0	9.0	10.0	11.0	15.0

Appendix D

RECORDS OF PILE TEST LOADING AND DRIVING

Table D - 1
RECORD OF PILE TEST LOADING
13th Day Static Load Test No. 1
Quick Test Load Method

County—Jefferson; Control—200-14-22; Project—U 1043(18) PD 974; Highway No.—US 69, etc.; Structure—S.H. 347 Overpass N. Bound Lane, # 86; Bent No.—3; Test Load Pile No.—3; Sta.—345+80.42; Rt.—12; Pile Size & Type—16" Metal Shell; Total Length—53'; Pile Tip Elevation—30.85; Design Load—45.7; Dynamic Resistance—25.1; Hammer Type & Size—Delmag—12; Time Test Began—12:45; Date—Dec. 20, 1966; S. W. Copp, Resident Engineer.

Total Elapsed Time Min.	Time Interval Min.	Load Added Tons	Total Load Tons	Extensometer Readings		Increase in Gross Settlement - Inches			Total Gross Settlement Inches
				Dial 1	Dial 2	Dial 1	Dial 2	Average Increase	
0	0	0	0	1.800	0.800	0	0	0	
	2.5	10	10	1.790	0.789	.010	.011	.011	.011
	0			1.791	0.790	+.001	+.001	+.001	.010
	2.5	10	20	1.778	0.779	.013	.011	.012	.022
	0			1.779	0.780	+.001	+.001	+.001	.021
	2.5	10	30	1.766	0.769	.013	.011	.012	.033
	0			1.767	0.770	+.001	+.001	+.001	.032
	2.5	10	40	1.752	0.757	.015	.013	.014	.046
	0			1.748	0.754	.004	.003	.004	.050
	2.5	10	50	1.735	0.743	.013	.011	.012	.062
	0			1.731	0.739	.004	.004	.004	.066
	2.5	10	60	1.713	0.723	.018	.016	.017	.083
	0			1.706	0.715	.009	.008	.008	.091
	2.5	10	70	1.684	0.694	.022	.021	.022	.113
	0			1.646	0.658	.038	.036	.037	.150
	1.5	Hold	70	1.097	0.120	.549	.538	.543	.693
	2.5	Hold	61	1.083	0.095	.014	.025	.020	.713
	2.5			1.180	0.186	+.097	+.091	+.094	.619
	2.5			1.185	0.189	+.005	+.003	+.004	.615
	2.5			1.185	0.189	.000	.000	.000	.615

Table D - 2
RECORD OF PILE TEST LOADING
13th Day Static Load Test No. 2
Quick Test Load Method

County—Jefferson; Control—200-14-22; Project—U 1043(18) Etc PD 974; Highway No.—US 69 etc. Structure—S.H. 347 Overpass N Bound Lane, # 86; Bent No.—3; Test Load Pile No.—3; Sta.—345+80.42; Rt.—12; Pile Size & Type—16" Metal Shell; Total Length—53; Pile Tip Elevation—30.5; Design Load—45.7; Dynamic Resistance—25.9; Hammer Type & Size—Delmag 12; Time Test Began—3:19; Date—Dec. 20, 1966; S. W. Copp, Resident Engineer.

Total Elapsed Time Min.	Time Interval Min.	Load Added Tons	Total Load Tons	Extensometer Readings		Increase in Gross Settlement - Inches			Total Gross Settlement Inches
				Dial 1	Dial 2	Dial 1	Dial 2	Average Increase	
0	0	0	0	1.700	0.800	0	0		
	2.5	10	10	1.692	0.789	.008	.011	.009	.009
	0			1.692	0.789	.000	.000	.000	.009
	2.5	10	20	1.683	0.778	.009	.011	.010	.019
	0			1.683	0.778	.000	.000	.000	.019
	2.5	10	30	1.676	0.766	.007	.012	.008	.027
	0			1.676	0.768	.000	+.002	.001	.028
	2.5	10	40	1.651	0.753	.025	.015	.020	.048
	0			1.653	0.752	+.002	+.001	+.001	.049
	2.5	10	50	1.646	0.740	.007	.012	.008	.053
	0			1.649	0.736	+.003	.004	.003	.060
	2.5	10	60	1.627	0.720	.022	.016	.019	.079
	0			1.608	0.715	.019	.005	.012	.091
	2.5	10	70	1.590	0.698	.018	.017	.017	.108
	0			1.580	0.688	.010	.010	.010	.118
		Hold	69	1.270	0.395	.310	.293	.301	.419
	2.5	Hold	67	1.264	0.372	.006	.023	.014	.433
	2.5	Hold	60	1.262	0.370	.002	.002	.002	.435
	2.5		0	1.363	0.464	+.101	+.094	+.097	.338
	2.5		0	1.365	0.467	.002	.003	+.002	.335
	2.5		0	1.366	0.467	.001	.000	+.001	.334
				.334	.333				

Table D - 3
RECORD OF PILE TEST LOADING
30th DAY STATIC LOAD TEST NO. 1

Load Tons	North Gage Inches	South Gage Inches	Total Gross Settlement Average Inches
0	0	0	0
10	.008	.008	.008
20	.020	.020	.020
30	.031	.032	.0315
40	.047	.050	.0485
50	.061	.067	.064
60	.081	.088	.0845
70	.099	.107	.103
80	.127	.132	.1295
85	.219	.228	.2235
85	.255	.265	.260
0	.249	.251	.251

Note: Time interval between each load increment was 2.5 minutes.

Table D - 4
RECORD OF PILE TEST LOADING
30th DAY STATIC LOAD TEST NO. 2

Load Tons	North Gage Inches	South Gage Inches	Total Gross Settlement Average Inches
0	0	0	0
10	.008	.008	.008
20	.019	.020	.0195
30	.029	.030	.0295
40	.044	.047	.0455
50	.056	.062	.059
60	.074	.081	.0775
70	.092	.101	.0965
80	.123	.132	.1275
85	.278	.287	.2825
89			

Note: The load dropped down to 80 tons, then after that brought to 85 tons. The dial started moving very fast; no reading could be taken.

Table D - 5
TEST PILE DRIVING DATA

County—Jefferson; Project—U 1043(18) etc; Highway No.—U.S. 69; Control—200-14-22 PD 974; Structure or Stream—SH 347 N. Bound Lane; Sta.—345+80.42; Rt. L. 12 Ft.; Design Brg. Resist.—45.7 Tons; Length—53 Ft. Steel Pile Size—16"; Ground Elevation—20.4; Weight of Hammer—2,750 Lbs.; Size and Make of Single Acting Power Hammer—Delmag 12; Stirling W. Copp, Resident Engineer. Date—Dec. 7, 1966.

Pile Tip Elevation (Ft.)	Depth of Pile in Ground	Speed & Stroke or Energy of Hammer	Number of Blows	Total Penetration (Inches)	Average Penetration (Inches)
	4"				
	5"				
	6'				
	7'				
	8'				
	9'				
	10'				
9.40	11'	11,000	10	12	1.20
8.40	12'	13,750	9	12	1.33
7.40	13'	13,750	9	12	1.33
6.40	14'	13,750	11	12	1.09
5.40	15'	13,750	12	12	1.00
4.90	6"	12,375	7	6	0.86
4.40	16'	13,750	6	6	1.00
3.90	6"	13,750	6	6	1.00
3.40	17'	12,375	6	6	1.00
2.90	6"	13,750	7	6	0.86
2.40	18'	13,750	6	6	1.00
1.90	6"	13,750	7	6	0.86
1.40	19'	13,750	8	6	0.75
0.90	6"	13,750	9	6	0.67
0.40	20'	13,750	10	6	0.60
- 0.10	6"	13,750	10	6	0.60
- 0.60	21'	13,750	10	6	0.60
- 1.10	6"	13,750	10	6	0.60
- 1.60	22'	13,750	10	6	0.60
- 2.10	6"	13,750	10	6	0.60
- 2.60	23'	13,750	10	6	0.60
- 3.10	6"	13,750	10	6	0.60
- 3.60	24'	13,750	10	6	0.60
- 4.10	6"	13,750	10	6	0.60
- 4.60	25'	13,750	10	6	0.60
- 5.10	6"	15,125	12	6	0.50
- 5.60	26'	13,750	13	6	0.46
- 6.10	6"	13,750	13	6	0.46
- 6.60	27'	13,750	12	6	0.50
- 7.10	6"	15,125	13	6	0.46
- 7.60	28'	15,125	13	6	0.46
- 8.10	6"	15,125	13	6	0.46
- 8.60	29'	15,125	19	6	0.32
- 9.10	6"	15,125	20	6	0.30
- 9.60	30'	15,125	20	6	0.30
- 9.85	3"	15,125	7	3	0.43

TEST PILE DRIVING DATA (Cont.)

Pile Tip Elevation (Ft.)	Depth of Pile in Ground	Speed & Stroke or Energy of Hammer	Number of Blows	Total Penetration (Inches)	Average Penetration (Inches)
-10.10	6"	15,125	8	3	0.38
-10.35	9"	15,125	8	3	0.38
-10.60	31'	15,125	7	3	0.43
-10.85	3"	13,750	7	3	0.43
-11.10	6"	13,750	6	3	0.50
-11.35	9"	13,750	6	3	0.50
-11.60	32'	13,750	6	3	0.50
-11.85	3"	13,750	6	3	0.50
-12.10	6"	13,750	6	3	0.50
-12.35	9"	12,375	6	3	0.50
-12.60	33'	12,375	6	3	0.50
-12.85	3"	12,375	6	3	0.50
-13.10	6"	12,375	6	3	0.50
-13.35	9"	12,375	6	3	0.50
-13.60	34'	13,750	5	3	0.60
-13.85	3"	12,375	6	3	0.50
-14.10	6"	13,750	5	3	0.50
-14.35	9"	12,375	5	3	0.60
-14.60	35'	13,750	5	3	0.60
-14.85	3"	13,750	5	3	0.60
-15.10	6"	12,375	6	3	0.50
-15.35	9"	12,375	6	3	0.50
-15.60	36'	13,750	5	3	0.60
-15.85	3"	13,750	5	3	0.60
-16.10	6"	13,750	6	3	0.50
-16.35	9"	13,750	6	3	0.50
-16.60	37'	13,750	6	3	0.50
-16.85	3"	13,750	5	3	0.60
-17.10	6"	13,750	5	3	0.60
-17.35	9"	13,750	5	3	0.60
-17.60	38'	12,375	5	3	0.60
-17.85	3"	13,750	5	3	0.60
-18.10	6"	13,750	5	3	0.60
-18.35	38' 9"	13,750	5	3	0.60
-18.60	39'	13,750	5	3	0.60
-18.85	39' 3"	13,750	5	3	0.60
-19.10	6"	13,750	5	3	0.60
-19.35	9"	13,750	5	3	0.60
-19.60	40'	13,750	5	3	0.60
-19.85	3"	12,375	5	3	0.60
-20.10	6"	12,375	5	3	0.60
-20.35	9"	13,750	5	3	0.60
-20.60	41'	12,375	5	3	0.60
-20.85	3"	13,750	6	3	0.50
-21.10	6"	13,750	5	3	0.60
-21.35	9"	13,750	5	3	0.60
-21.60	42'	13,750	6	3	0.50
-21.85	3"	12,375	5	3	0.60
-22.10	6"	13,750	5	3	0.60
-22.35	9"	13,750	5	3	0.60
-22.60	43'	12,375	5	3	0.60
-22.85	3"	13,750	6	3	0.50
-23.10	43' 6"	13,750	5	3	0.60
-23.35	9"	13,750	6	3	0.50
-23.60	44'	12,375	5	3	0.60
-23.85	3"	12,375	5	3	0.60
-24.10	6"	13,750	5	3	0.60
-24.35	9"	13,750	5	3	0.60
-24.60	45'	12,375	6	3	0.50
-24.85	3"	12,375	5	3	0.60
-25.10	6"	12,375	6	3	0.50
-25.35	9"	13,750	5	3	0.60
-25.60	46'	13,750	5	3	0.60
-25.85	3"	13,750	5	3	0.60
-26.10	6"	13,750	6	3	0.50
-26.35	9"	12,375	6	3	0.50
-26.60	47'	12,375	6	3	0.50
-26.85	3"	13,750	6	3	0.50
-27.10	6"	13,750	5	3	0.60
-27.35	9"	12,375	6	3	0.50
-27.60	48'	12,375	6	3	0.50
-27.85	48' 3"	12,375	6	3	0.50
-28.10	6"	13,750	6	3	0.50
-28.35	9"	13,750	6	3	0.50
-28.60	49'	13,750	6	3	0.50
-28.85	3"	13,750	6	3	0.50
-29.10	6"	13,750	7	3	0.43

TEST PILE DRIVING DATA (Cont.)

Pile Tip Elevation (Ft.)	Depth of Pile in Ground	Speed & Stroke or Energy of Hammer	Number of Blows	Total Penetration (Inches)	Average Penetration (Inches)
-29.35	9"	13,750	7	3	0.43
-29.60	50'	13,750	7	3	0.43
-29.85	3"	13,750	7	3	0.43
-30.10	6"	13,750	7	3	0.43
-30.35	9"	13,750	7	3	0.43
-30.60	51'	13,750	7	3	0.43
-30.85	3"	13,750	7	3	0.43

Appendix E COMPUTER SIMULATION

1/DELTA T		P	EXP. PRESSURE		TIME INTERVAL N = 1ACC. OF M,P) = -1.0 G				
23247.8		14	93700.		SEGMENT M	STRESS(M)	F(M)	R(M)	V(M)
M	W(M)	K(M)	AREA(M)	RU(M)					
1	2750.000	0.3120000E 08	109.000	-0.	1	2330.	254000.	0.	15.645317
2	754.000	0.7000000E 08	258.000	-0.	2	3.	754.	-0.	0.466155
3	200.000	0.9450000E 07	21.500	-0.	3	44.	954.	-0.	-0.000000
4	321.000	0.9450000E 07	18.900	-0.	4	67.	1275.	-0.	0.000000
5	321.000	0.9450000E 07	18.900	-0.	5	84.	1596.	-0.	-0.000000
6	321.000	0.9450000E 07	18.900	105300.000	6	63.	1190.	727.	-0.
7	321.000	0.9450000E 07	18.900	80599.999	7	51.	955.	556.	-0.000000
8	321.000	0.9450000E 07	18.900	65000.000	8	44.	828.	449.	-0.000000
9	321.000	0.9450000E 07	18.900	100099.999	9	24.	458.	691.	-0.000000
10	321.000	0.9450000E 07	18.900	48099.999	10	24.	447.	332.	-0.000000
11	321.000	0.9450000E 07	18.900	38350.000	11	27.	504.	265.	0.000000
12	321.000	0.9450000E 07	18.900	50700.000	12	25.	475.	350.	-0.
13	321.000	0.9450000E 07	18.900	44849.999	13	26.	486.	309.	0.000000
14	321.000	0.7215000E 07	18.900	44849.999	14	26.	498.	309.	-0.
15	-0.	-0.	-0.	72149.999					

ENERGY		HAMMER EFFICIENCY		RU(TOTAL)	
22600.00		0.47		650000.0	
Q(POINT)	Q(SIDE)	J(POINT)	J(SIDE)		
0.01	0.01	0.	0.		
OPTIONS	1	2	3	4	11 12 13 14 15
	2	2	1	1	2 3 0 1 2
SLACK(M)	ERES(M)	VSTART(M)	KPRIME(M)		
1000.000	1.00	15.77	-0.		
1000.000	1.00	0.	-0.		
1000.000	1.00	0.	-0.		
0.	1.00	0.	-0.		
0.	1.00	0.	-0.		
0.	1.00	0.	0.1053000E 08		
0.	1.00	0.	0.8060000E 07		
0.	1.00	0.	0.6500000E 07		
0.	1.00	0.	0.1001000E 08		
0.	1.00	0.	0.4810000E 07		
0.	1.00	0.	0.3835000E 07		
0.	1.00	0.	0.5070000E 07		
0.	1.00	0.	0.4485000E 07		
1000.000	1.00	0.	0.4485000E 07		
-0.	-0.	-0.	0.		

TIME INTERVAL N = 11ACC. OF M,P) = -1.0 G					
SEGMENT M	STRESS(M)	F(M)	R(M)	V(M)	
1	12284.	1338947.	0.	9.953360	
2	1780.	459117.	-0.	15.695932	
3	11434.	245837.	-0.	16.015492	
4	1191.	22512.	-0.	2.939337	
5	128.	2412.	-0.	0.184276	
6	64.	1207.	746.	0.005702	
7	51.	956.	556.	0.000104	
8	44.	828.	449.	0.000001	
9	24.	458.	691.	0.000000	
10	24.	447.	332.	0.000000	
11	27.	504.	265.	0.000000	
12	25.	475.	350.	0.000000	
13	26.	486.	309.	0.000000	
14	26.	498.	309.	0.000000	

TIME INTERVAL N = 21ACC. OF M,P) = -1.0 G				
SEGMENT M	STRESS(M)	F(M)	R(M)	V(M)
1	860.	93700.	0.	7.144643
2	1927.	497056.	-0.	16.014836
3	30853.	663336.	-0.	17.309402
4	20521.	387847.	-0.	17.669627
5	4911.	92809.	-0.	6.773836
6	593.	11212.	12727.	1.060461
7	88.	1668.	1194.	0.101976
8	46.	862.	473.	0.006388
9	24.	459.	692.	0.000273
10	24.	447.	332.	0.000009
11	27.	504.	265.	0.000000
12	25.	475.	350.	0.000000
13	26.	486.	309.	0.000000
14	26.	498.	309.	0.000000

TIME INTERVAL N = 61ACC. OF M,P) = 3.3 G				
SEGMENT M	STRESS(M)	F(M)	R(M)	V(M)
1	860.	93700.	0.	5.314020
2	1103.	284502.	-0.	1.339715
3	11340.	243811.	-0.	3.050996
4	15034.	284142.	-0.	1.936657
5	19383.	366335.	-0.	2.778942
6	12595.	238040.	105300.	2.710955
7	21732.	410735.	80600.	2.947291
8	31491.	595182.	65000.	11.647194
9	17301.	326988.	100100.	12.673159
10	5820.	109997.	48100.	5.406745
11	1833.	34639.	18508.	1.777888
12	484.	9148.	6154.	0.520087
13	121.	2283.	1328.	0.126839
14	40.	764.	475.	0.024872

TIME INTERVAL N = 31ACC. OF M,P) = -1.0 G				
SEGMENT M	STRESS(M)	F(M)	R(M)	V(M)
1	860.	93700.	0.	6.686987
2	1174.	302909.	-0.	9.400656
3	19355.	416217.	-0.	11.417687
4	34697.	655771.	-0.	15.287300
5	28936.	546900.	-0.	18.792783
6	8365.	158093.	105300.	8.647637
7	1668.	31533.	30523.	2.185938
8	263.	4975.	3583.	0.387751
9	44.	839.	1125.	0.044823
10	25.	474.	346.	0.003880
11	27.	505.	265.	0.000250
12	25.	475.	350.	0.000012
13	26.	486.	309.	0.000000
14	26.	498.	309.	0.000000

TIME INTERVAL N = 71ACC. OF M,P) = 25.9 G				
SEGMENT M	STRESS(M)	F(M)	R(M)	V(M)
1	860.	93700.	0.	4.856364
2	1099.	283531.	-0.	-0.679822
3	9871.	212237.	-0.	0.795673
4	15105.	285479.	-0.	0.124192
5	16313.	308311.	-0.	0.174662
6	16546.	312720.	105300.	0.972102
7	9524.	179998.	80600.	1.000892
8	14222.	268798.	65000.	-0.285391
9	25645.	484686.	100100.	8.004917
10	20056.	379053.	48100.	12.654022
11	8266.	156235.	38350.	7.070445
12	2596.	49061.	36560.	2.364953
13	783.	14806.	9282.	0.767717
14	212.	4000.	2486.	0.223049

TIME INTERVAL N = 41ACC. OF M,P) = -1.0 G				
SEGMENT M	STRESS(M)	F(M)	R(M)	V(M)
1	860.	93700.	0.	6.229331
2	937.	241679.	-0.	6.177866
3	13133.	282350.	-0.	7.929543
4	20290.	383484.	-0.	7.128066
5	35987.	680164.	-0.	10.943426
6	30751.	581186.	105300.	17.549968
7	11690.	220942.	80600.	10.613143
8	3106.	58712.	48971.	3.271411
9	596.	11265.	14100.	0.758396
10	111.	2094.	1275.	0.143927
11	37.	692.	348.	0.019922
12	26.	491.	359.	0.002040
13	26.	487.	310.	0.000163
14	26.	498.	309.	0.000011

TIME INTERVAL N = 81ACC. OF M,P) = 92.6 G				
SEGMENT M	STRESS(M)	F(M)	R(M)	V(M)
1	5058.	551374.	0.	3.552960
2	1577.	406810.	-0.	0.273045
3	9776.	210189.	-0.	0.381641
4	13471.	254605.	-0.	-2.238245
5	17127.	323692.	-0.	-1.519580
6	12260.	231718.	60286.	-1.305932
7	13099.	247565.	80587.	-0.417534
8	7396.	139785.	51353.	0.928321
9	5156.	97441.	77587.	-2.090317
10	20513.	387693.	48100.	3.970747
11	22145.	418541.	38350.	11.267416
12	10470.	197887.	50700.	8.284528
13	3533.	66774.	44850.	3.059408
14	1208.	22840.	14198.	1.025791

TIME INTERVAL N = 51ACC. OF M,P) = -0.8 G				
SEGMENT M	STRESS(M)	F(M)	R(M)	V(M)
1	860.	93700.	0.	5.771676
2	1000.	257965.	-0.	3.644726
3	11884.	255511.	-0.	5.453908
4	17421.	329264.	-0.	4.194304
5	18803.	355369.	-0.	4.536760
6	28642.	541338.	105300.	6.878000
7	31448.	594361.	80600.	15.398893
8	15838.	299343.	65000.	12.157813
9	4133.	78122.	100100.	3.905509
10	1122.	21211.	13556.	1.216318
11	261.	4924.	2382.	0.311408
12	62.	1175.	778.	0.058949
13	30.	574.	355.	0.008647
14	27.	505.	314.	0.001012

TIME INTERVAL N = 91ACC. OF M,P) = 397.5 G				
SEGMENT M	STRESS(M)	F(M)	R(M)	V(M)
1	4093.	446126.	0.	0.497084
2	2116.	545941.	-0.	4.503495
3	18923.	406835.	-0.	4.597907
4	15654.	295852.	-0.	0.279833
5	12521.	236655.	-0.	-2.526639
6	13728.	259462.	20884.	-0.887602
7	8852.	167294.	26763.	-0.844315
8	9272.	175233.	58574.	-1.284877
9	5922.	111922.	58221.	1.513010
10	857.	16206.	12317.	-2.483296
11	14557.	275137.	38350.	0.010642
12	21480.	405964.	50700.	8.751993
13	12942.	244608.	44850.	8.935344
14	3817.	72150.	44850.	3.872184

TIME INTERVAL N = 101ACC. OF M.P) = 576.9 G
 SEGMENT M STRESS(M) F(M) R(M) V(M)

1	860.	93700.	0.	-0.385146
2	1828.	471699.	-0.	0.338387
3	20246.	435296.	-0.	0.152023
4	22847.	431815.	-0.	4.408022
5	15003.	283564.	-0.	3.279450
6	11012.	208134.	-41469.	0.084391
7	11415.	215746.	22815.	-0.147336
8	7079.	133794.	22063.	0.159968
9	5354.	101190.	45889.	-2.149388
10	7331.	138550.	11853.	1.313842
11	-662.	-12517.	-11690.	-1.619244
12	7260.	137213.	42139.	-2.980356
13	15989.	302188.	44850.	6.044829
14	3817.	72150.	44850.	12.731832

SEGMENT	AREA	TIME N	MAX C STRESS
1	109.000	9	12952.
2	258.000	18	2475.
3	21.500	21	30853.
4	18.900	29	35285.
5	18.900	37	38889.
6	18.900	45	35368.
7	18.900	53	32679.
8	18.900	61	31491.
9	18.900	69	26780.
10	18.900	76	24708.
11	18.900	84	23491.
12	18.900	91	21480.
13	18.900	97	18536.
14	18.900	210	3817.

TIME INTERVAL N = 111ACC. OF M.P) = -1028.9 G
 SEGMENT M STRESS(M) F(M) R(M) V(M)

1	1138.	124075.	0.	-0.858367
2	1034.	266882.	-0.	-2.909454
3	10471.	225117.	-0.	-3.709494
4	18333.	346494.	-0.	1.065100
5	21671.	409573.	-0.	5.346507
6	17162.	324353.	90903.	4.035685
7	10641.	201110.	25013.	1.513043
8	9183.	173553.	33902.	0.063309
9	5810.	109813.	22006.	1.730137
10	3717.	70243.	-4012.	-1.790226
11	7431.	140454.	3381.	1.269688
12	-5463.	-103258.	-20007.	2.045619
13	-11284.	-213271.	44850.	0.926835
14	3817.	72150.	44850.	9.215815

TIME N	MAX T STRESS	DMAX (M)
387	-0.	0.310567
387	-0.	0.311323
387	-0.	0.305898
353	7866.	0.276058
341	5529.	0.252125
192	2324.	0.214693
305	3358.	0.187588
178	1503.	0.176111
343	1401.	0.164203
164	4831.	0.162000
125	6470.	0.148422
110	5531.	0.145772
115	16343.	0.139935
374	-0.	0.138240

PERMANENT SET OF FILE = 0.12824012 INCHES

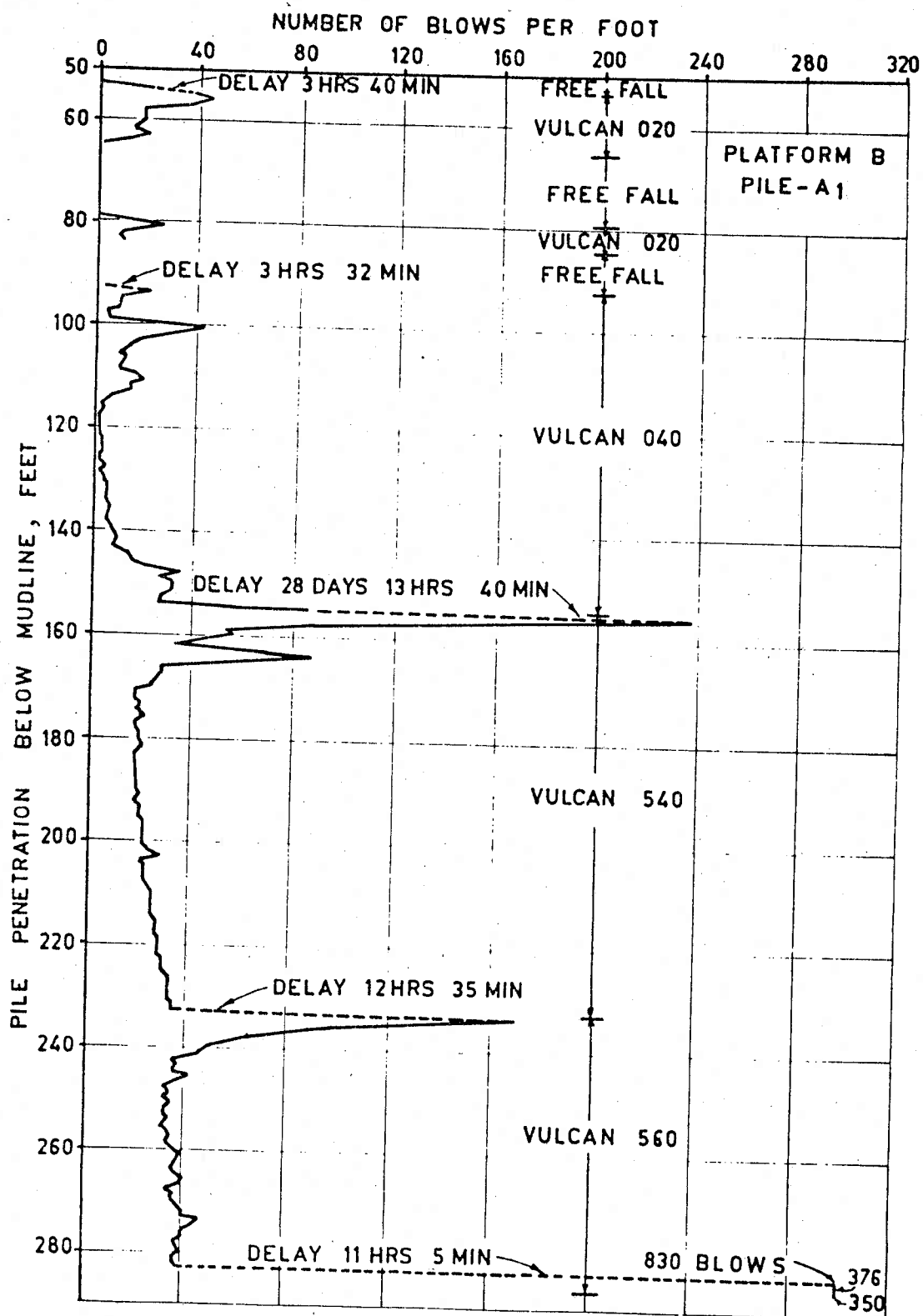


Fig. 10 - Typical pile driving record.

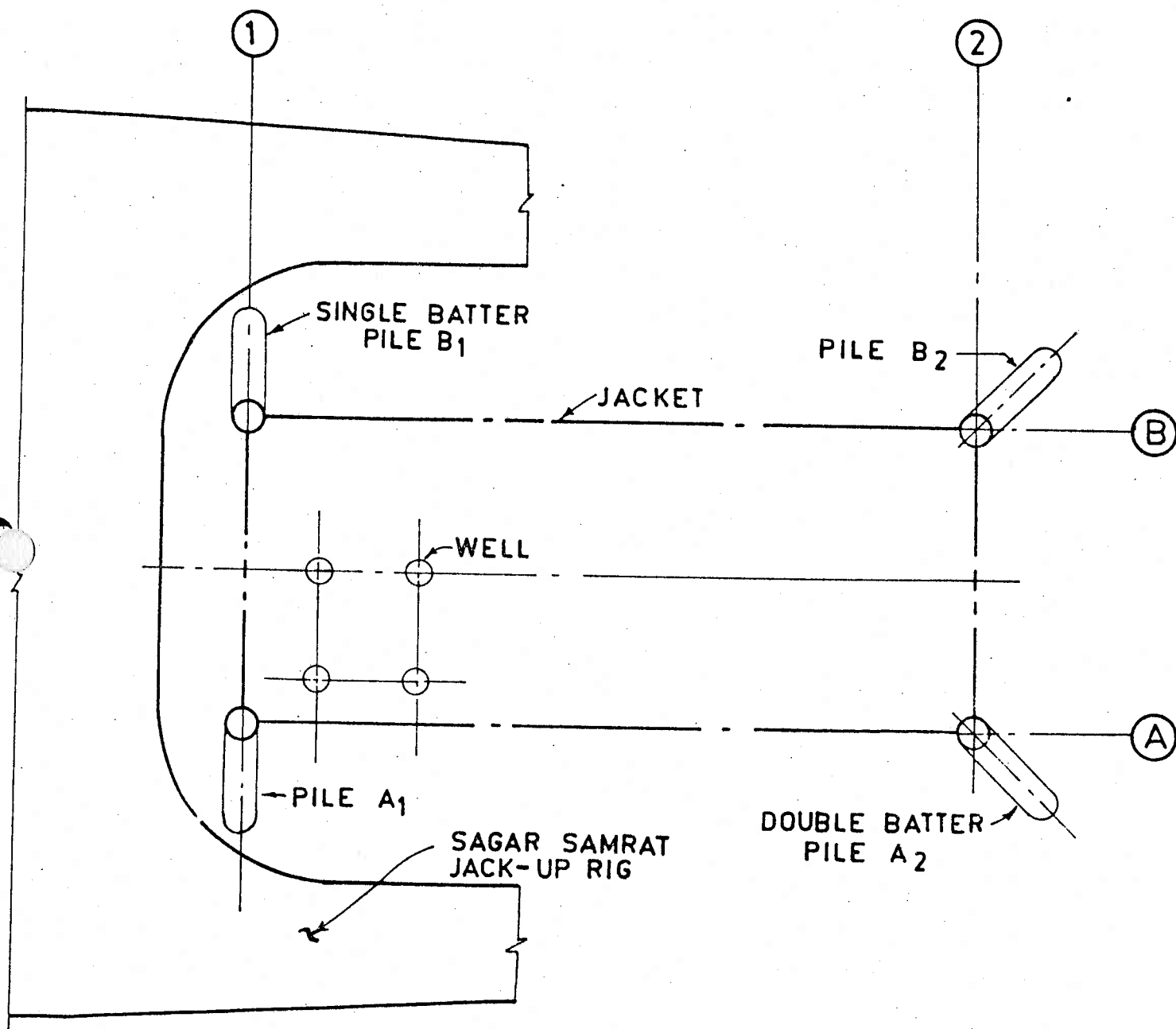


Fig. 9 - Orientation of jack up rig and jacket.

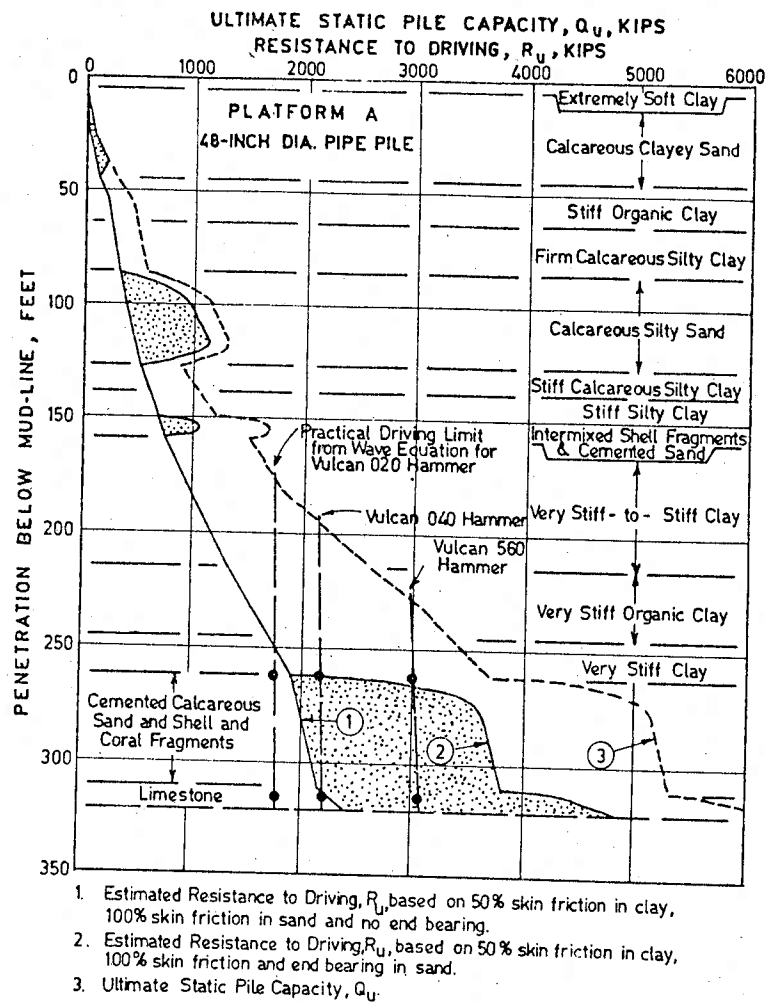


FIG. 7 - INTERPRETATION OF PILE DRIVABILITY.

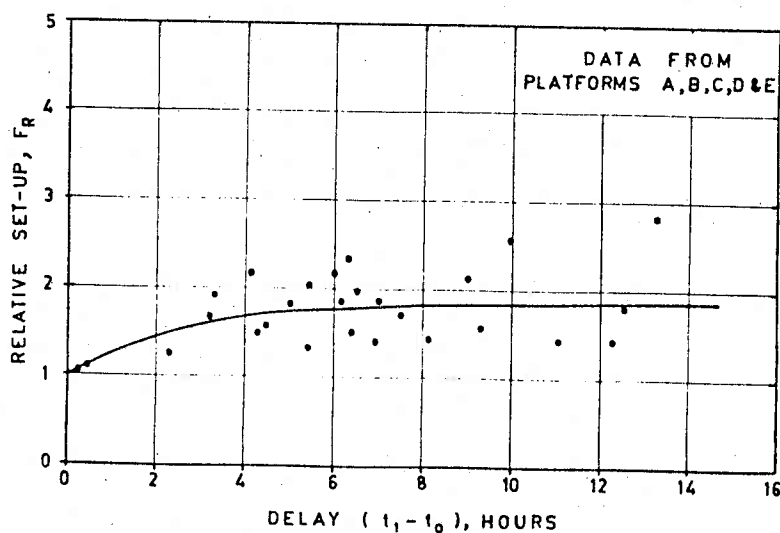


FIG. 8 - RELATIONSHIP BETWEEN DELAY AND RELATIVE SOIL SET-UP.

HAMMER PARAMETERS			
Hammer Properties	Vulcan 020	Vulcan 040	Vulcan 560
Rated Energy, ft-lb	60,000	120,000	300,000
Weight of Ram, lb	20,000	40,000	62,500
Drop, ft	3	3	5
Efficiency, %	75	75	75
Weight of Pile Cap, lb	5,000	27,800	48,000
Cushion	2 pieces asbestos 1/4-in. thick alternating with 1 piece steel plate 1/4-in. thick		
Cushion Spring Constant, lb/in.	3.4×10^6	2.78×10^6	4.14×10^6
Coefficient of Restitution:			
Cushion	0.6	0.6	0.6
Pile Cap	0.9	0.9	0.9
PILE PARAMETERS			
Pile Properties	Penetration, Ft		
	261	315	
Total Pile Length, ft	586	586	
Pile Diameter, in.	48	48	
Wall Thickness	See Fig. 5	See Fig. 5	
Modulus of Elasticity, psi	29.6×10^6	29.6×10^6	

SOIL PARAMETERS

Soil Properties	Penetration, Ft	
	261	315
Quake, in.		
Side	0.1	0.1
Tip	0.1	0.1
Damping, sec/ft		
Side	0.18	0.17
Tip	0.15	0.15

FIG. 4 - WAVE EQUATION PARAMETERS FOR PLATFORM A.

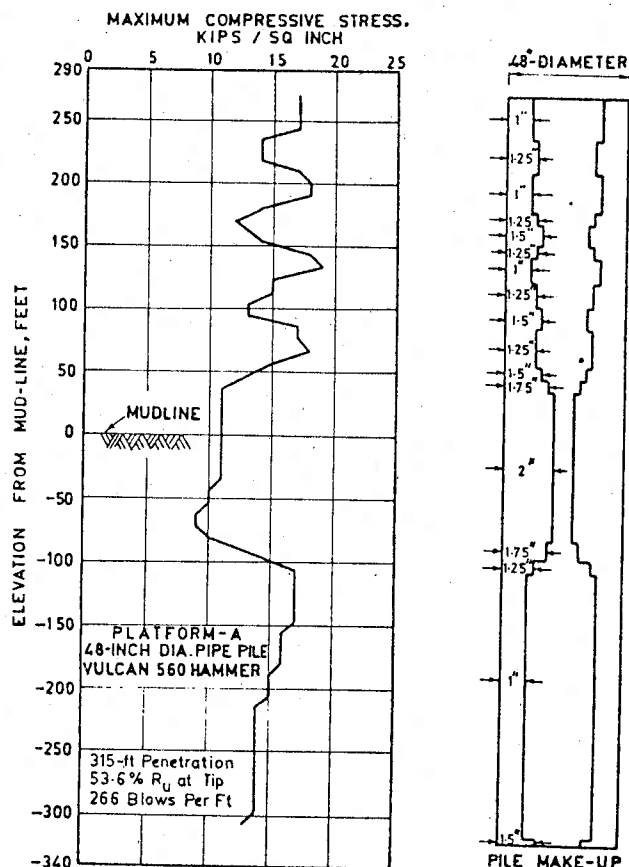


FIG. 5 - PILE MAKE-UP AND COMPUTED MAXIMUM COMPRESSIVE STRESS.

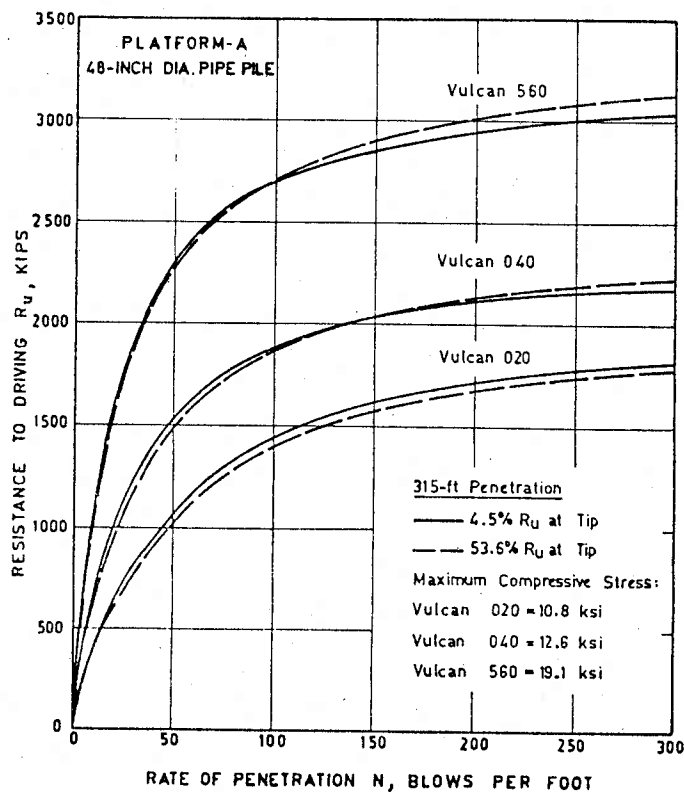


FIG. 6 - RESULTS OF WAVE EQUATION ANALYSIS.

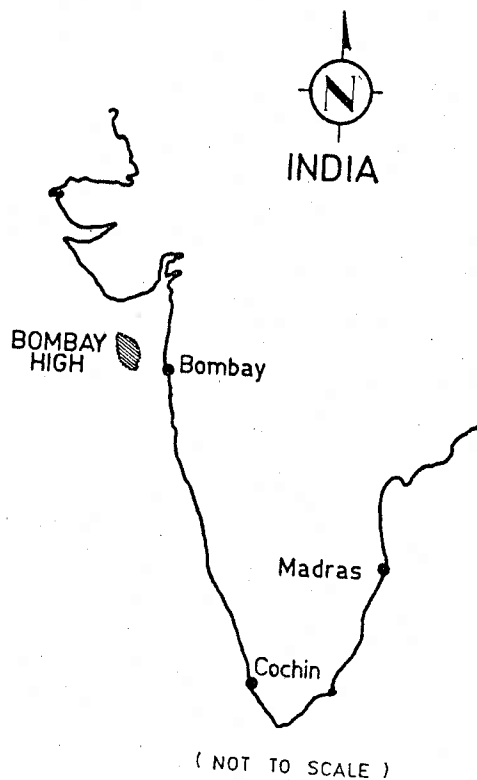


FIG. 1 - SITE LOCATION OF BOMBAY HIGH FIELD.

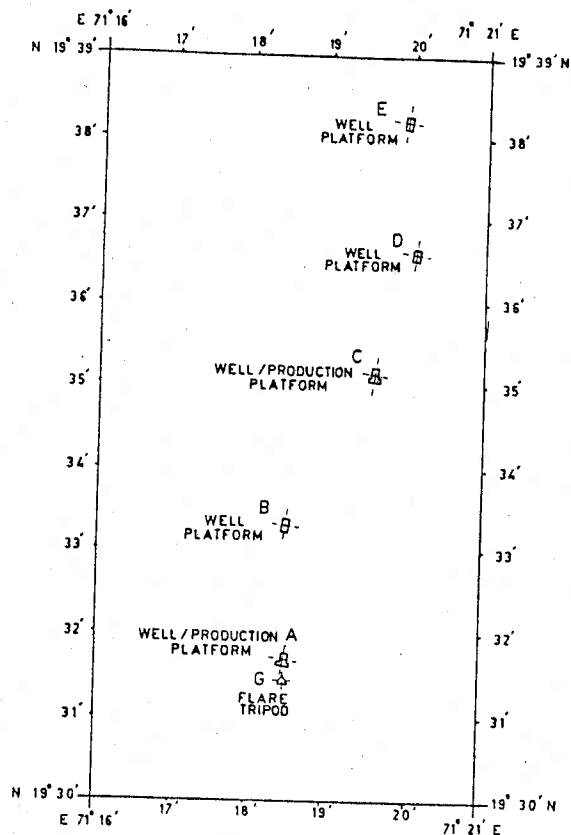


FIG. 2 - PLATFORMS LAYOUT.

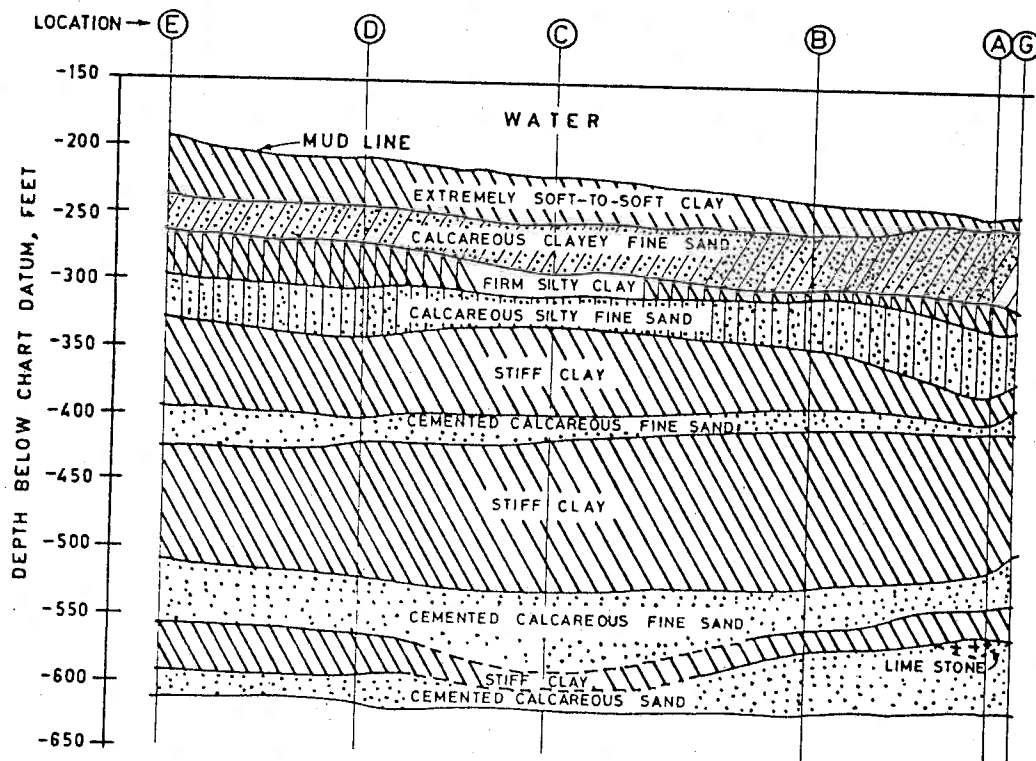


FIG. 3 - GENERALIZED SOIL PROFILE.